AD-A169 793 CAVITATION INCEPTION(U) CALIFORNIA INST OF TECH PASADENA DIV OF ENGINEERING AND APPLIED SCIENCE A J ACOSTA 31 JAN 86 E183.8 N00014-85-K-0073 1/1

UNCLASSIFIED F/G 20/4 NL

END
DATE FILMED
8-86

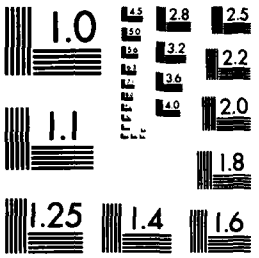

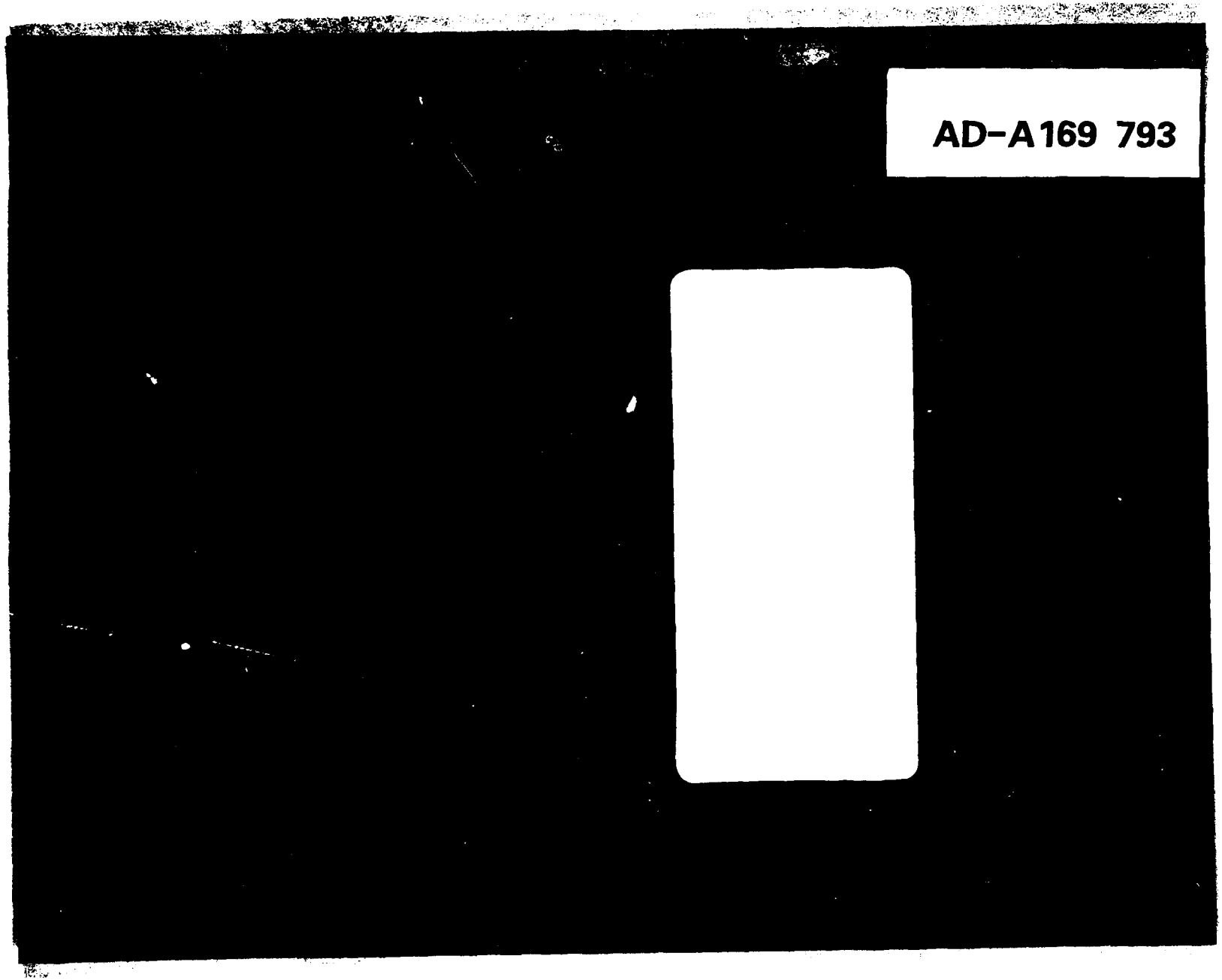
AD-A169 793

(1)

CAVITATION INCEPTION

BY A. J. ACOSTA

REPORT NO. E183.8 JANUARY 1986

CONTRACT N00014-85-K-0073

FINAL REPORT

UNCLASSIFIED

SECURITY CLASSIFICATION OF THIS PAGE

REPORT DOCUMENTATION PAGE

1a. REPORT SECURITY CLASSIFICATION: UNCLASSIFIED	1b. RESTRICTIVE MARKINGS: N/A
2a. SECURITY CLASSIFICATION AUTHORITY: N/A	3. DISTRIBUTION/AVAILABILITY OF REPORT: APPROVED FOR PUBLIC RELEASE; DISTRIBUTION UNLIMITED
2b. DECLASSIFICATION/DOWNGRADING SCHEDULE: N/A	
4. PERFORMING ORGANIZATION REPORT NUMBER(S): E183.8	5. MONITORING ORGANIZATION REPORT NUMBER(S)
6a. NAME OF PERFORMING ORGANIZATION: California Institute of Technology; 6b. OFFICE SYMBOL (If applicable)	7a. NAME OF MONITORING ORGANIZATION: DAVID W. TAYLOR NAVAL SHIP RESEARCH AND DEVELOPMENT CENTER, Code 1504 (1505)
6c. ADDRESS (City, State, and ZIP Code): Pasadena, CA 91125	7b. ADDRESS (City, State, and ZIP Code): BETHESDA, MARYLAND 20084-5000
8a. NAME OF FUNDING/SPONSORING ORGANIZATION: Naval Sea Systems Command; 8b. OFFICE SYMBOL (If applicable): SEA 05R24	9. PROCUREMENT INSTRUMENT IDENTIFICATION NUMBER: Contract Number - N00014-85-K-0073
8c. ADDRESS (City, State, and ZIP Code): Washington, D. C. 20360	10. SOURCE OF FUNDING NUMBERS: PROGRAM ELEMENT NO: 61153N; PROJECT NO: SR 023 01; TASK NO: 23454; WORK UNIT ACCESSION NO: N/A

11. TITLE (Include Security Classification): CAVITATION INCEPTION

12. PERSONAL AUTHOR(S): A. J. ACOSTA

13a. TYPE OF REPORT	13b. TIME COVERED	14. DATE OF REPORT (Year, Month, Day)	15. PAGE COUNT
FINAL	FROM 10/1/84 TO 9/30/85	1986, JANUARY 31	78

16. SUPPLEMENTARY NOTATION: Sponsored under the Naval Sea Systems Command General Hydromechanics Research (GHR) Program administered by the David W. Taylor Naval Ship R&D Center, Code 1504(1505), Bethesda, Maryland 20084-5000

17. COSATI CODES			18. SUBJECT TERMS (Continue on reverse if necessary and identify by block number)
FIELD	GROUP	SUB-GROUP	(U) GHR Program
20	04		

19. ABSTRACT (Continue on reverse if necessary and identify by block number)

This report summarizes work carried out on cavitation inception during the period 1984-1985. The work is experimental and is devoted to observation of cavitation past a bluff body, and in a separate effort to the development of a cavitation susceptability meter based on a venturi meter with detection of bubbles being done optically. The shear flow cavitation reveals the secondary vortex structure that has been of great interest in recent turbulence work, and it is within this secondary structure that cavitation commences. The major components of the susecptability meter and their design are described in detail although data have not as yet been taken.

20. DISTRIBUTION/AVAILABILITY OF ABSTRACT: ☒ UNCLASSIFIED/UNLIMITED ☐ SAME AS RPT ☐ DTIC USERS	21. ABSTRACT SECURITY CLASSIFICATION: UNCLASSIFIED
22a. NAME OF RESPONSIBLE INDIVIDUAL: Mr. V. J. Monacella	22b. TELEPHONE (Include Area Code): 202-227-1503; 22c. OFFICE SYMBOL: Code 1504/1505

DD FORM 1473, 84 MAR — 83 APR edition may be used until exhausted. All other editions are obsolete.

SECURITY CLASSIFICATION OF THIS PAGE: UNCLASSIFIED

CAVITATION INCEPTION

Final Report

Contract N00014-85-K-0073
David W. Taylor Naval Ship Research
and Development Center
Bethesda, Maryland 20034

Report E183.8

Prepared by

A. J. Acosta

California Institute of Technology
Division of Engineering and Applied Science
Pasadena, California 91125

January 1986
Report E183.8

1. INTRODUCTION

This report summarizes work carried out on Cavitation Inception under the auspices of the General Hydrodynamic Research program of the David W. Taylor Naval Ship Research and Development Center throughout the fiscal research year of 1985. This work is experimental in character and during the contract period was devoted to two principal areas. These were:

(a) Observations and analysis of cavitation past a bluff body,

(b) the design and implementation of a Cavitation Susceptibility Meter (CSM)

This has been an extremely busy period of development of means and procedures in both research activities as both represent fairly difficult experimental objectives. In what follows we describe the personnel involved and then the technical progress made and the probable direction of future work in this area.

2. PERSONNEL

Professors A. J. Acosta and R. H. Sabersky serve as principal investigators. Graduate students Timothy J. O'Hern and Luca d'Agostino are each supported in part by the contract. We also, on occasion, engage undergraduates to help in the laboratory; R. Arrieta, R. Moberly (freshman) and E. Morss (senior) were so engaged. Messrs. O'Hern and d'Agostino are expected to complete their graduate work during the summer of 1986. A new student Sheldon Green has joined our group as a 2nd year graduate student; he began under the aegis of the present contract (and continuing throughout fiscal 1986) a preliminary series of experiments on cavitation inception past a NACA 66-209 hydrofoil. This foil is the same one used previously in the two-dimensional working section of the High Speed Water Tunnel except that it is here mounted in the Low Turbulence Water Tunnel on a reflection-plane base giving it an

effective aspect ratio of about 2. A highly interesting and complex structure of tip-vortex cavitation results from this squared-off foil which will be reported elsewhere.

3. DISCUSSION

Equipment and facility.

Our primary laboratory is the Low Turbulence Water Tunnel (LTWT) sited in the Keck Laboratory of Hydraulics and Water Resources. Over some years with a variety of funding sources from the Department of the Navy and the Institute this water tunnel has been developed into a most inexpensive to use yet economic and versatile test facility. This together with our other major research equipment item, the holographic camera, are all described in Ref.1. In addition to that we have been deeply engaged in the construction of a cavitation susceptibility meter based upon the principal of the venturi tube as used by Gowing and Shen at DTNSRDC with data events being recorded optically rather than acoustically. (This approach we think suitable for a laboratory device rather than a field serviceable unit.) To this end a prototypical glass venturi tube, backscatter laser velocimeter and cavitation event and velocimeter data acquisition system has been designed in association with Shapiro Scientific Instruments of Costa Mesa, California and was delivered to us during the contract year. This device, the software programs necessary to operate it, the supporting circuitry are all described in a subsequent section.

Bluff body cavitation research

We have over the years been much concerned with cavitation inception in flows dominated by a large-scale laminar separation; typically these are flows characterized by either a forward facing or backward facing step; the simplest of these is just the classic flat plate set normally to the flow. The overall time-average behavior of this particular flow has been studied throughout the

present century for knowledge of the drag coefficient, base pressure, size and proportions of the time-average separation or recirculation zone. But it is only quite recently that we have begun to see more detailed studies of these kinds of flows in the context of cavitation inception and much of work referred to in Ref.1 is precisely that.

Cavitation inception in these "bluff" body flows occurs in the shear layer of the laminar separation region. This shear layer has been the sine-qua-non of much of the research into the organized structures of turbulence. It is interesting that cavitation inception studies in shear layers have been made over a number of years and the vortical nature of this cavitating flow was noted from the outset by many workers. These include, for example, Theodorsen, and later Parkin & Kermeen[1], and Hoyt[2], but it was not until the work Katz and O'Hern (Ref.25 of Ref.1) that the more delicate structure of these bluff body flows with cavitation became more clear. This brings us to the state of our present work in this topic:

The LTWT has been previously described at length (see Ref.1). In brief it is a non-resorber closed, return circuit water tunnel with provision for turbulence control and dissolved air content control. Maximum working section speed is about 7m/s. The working section is one foot square; it has plate glass windows that are useful for optical flow observation. Static pressure can be controlled by application of vacuum and a small (1/3 atm) positive pressure. A schematic of the bluff "test body" is shown in Fig.1. Flash photographs of cavitation in the flow past this test body are shown in Figs.2a,b. These reveal the important feature of this flow that makes it so interesting yet difficult for the prediction of cavitation inception. Shown there are simultaneous top and side photographs of the free shear layer in the flow past

1. See e.g. Knapp et al, Cavitation, 1970, p.233

2. Cavitation and Multiphase Flow Symposium, 1985, ASME.

first at inception and then with more developed cavitation. The inception index is quite high, about 1.5. There we see inception developing in an axially oriented vortex structure. With more developed cavitation the full pattern of this flow is revealed with the growing pattern of spanwise vorticity and the associated development of the secondary structure of vorticity.[1] It is extremely curious that this secondary streamwise vorticity is the cause of cavitation inception and so far the reasons for this are not yet clear.

It was in an effort to begin to understand this inception process that doubly-pulsed holograms were made of this cavitating flow. The experimental arrangement is shown in Fig.3 and the holocamera itself in Fig.4. Two holograms are made on one plate with an adjustable time delay of 10 to 500 microseconds. If the two images are recorded with nearly the same intensity, two images of objects or microbubbles can be reconstructed showing the displacement with the known time delay. This reconstruction is simply done as shown in Figs.5&6. Examples of these cavitating axial vortex structures are shown in Fig.7 where the two images are shown somewhat displaced. From holograms of this sort the three dimensional velocity field of the motion of particles can be deduced. Extensive samples of these kinds of results are tabulated in Table I. It was initially hoped that there would be an abundant supply of micronuclei surrounding these cavitating vortex structures so that a good idea of the vorticity or even the circulation around particular vortex cores could be established. This has so far not been possible because too few microbubbles were found near the core to deduce the necessary velocity field around the core. It is interesting to note however that this axial vorticity typically is found where the local streamwise speed is about 1/2 freestream value and that there all velocity

1. see for example L. Bernal "The Coherent Structure of Turbulent Mixing Layers, I. Similarity of the Primary Vortex Structure, "I. Secondary Streamwise Vortex Structure", Ph.D. Thesis 1981, Graduate Aeronautical Laboratories, California Institute of Technology.

components are on occasion equal in magnitude.

Cavitation inception indices are shown in Fig.8 for two different air contents; these are strikingly different indicating a pronounced effect of microbubble concentration (by inference). These findings are compared with earlier works on similar bluff bodies in Fig.9. By inspection of these (in particular the original work of Kermeen and Parkin (1957) and more recent work of Katz (1981)) secondary or axial vortices are apparent. Theories of cavitation inception based only on the concept of primary vortex roll-up cannot therefore be correct.

Thus it is their role in cavitation that our attention has been inevitably drawn to the role of these secondary structures in bluff body flows. To observe the connection between the two structures more clearly, motion picture strips have been made both of the cavitation inception process and more developed cavitation at about 2000 frames per second. These are most illustrative of the basic process and clearly show the linkage of the primary and secondary structures as time evolves. Still sections from such a movie are reproduced in Fig.10a,b to show this connection. Movies such as this are now in the process of being analyzed for the descriptive features of these flows; we hope to clarify these relationships in the very near future and in particular to deduce the intensity of the pressure fluctuations there causing cavitation. This has started in a preliminary way with the analysis of photographs such as those of Fig.2a. In this it is assumed the vortex core is at vapor pressure; then following ideas of Kermeen & Parkin (1957) one can estimate, roughly, the circulation around these vortex cores by assuming the vortical motion is that of a Rankine vortex. This, together with the known inception index and the observation of the core radius, enables one to make the estimate for the circulation of these secondary vortices

$$\Gamma_s = 2\pi r_c U(\sigma_i/2)^{1/2}$$

where Γ_s is the secondary vorticity, r_c the observed radius of the vortex core, U the reference speed for the calculation of the inception index σ_i. This reference is taken to be the flow velocity just outside the shear layer. Estimates of the spanwise or primary vorticity and circulation Γ_p have been made by many workers (ibid Bernal) and from this Table II has been prepared for several of the present data points[4]. It can be seen there that the ratio of the secondary to primary vorticity is small being for the most part less than 10 percent. Nevertheless, the pressure within the secondary vortex is less because of the much smaller size of the vortex core radius. The reasons for this difference are not known; it is interesting to speculate that this secondary flow structure is susceptible to Reynolds number scaling whereas this does not seem to be so for the resulting pressure coefficient of the primary circulation, as argued by Katz[5] and others.

Cavitation Susceptibility Meter (CSM)

This has been a major investment of our project and has required a rather more detailed and careful engineering enterprise than we at first thought.

The C.S.M. currently under development at Caltech is meant to be used in general for testing of any water source with pressure in the range 0 to 2 bar. Fig. 15 shows a general view of the experimental set-up. A typical application of the C.S.M. to the measurement of water quality in the low turbulence water tunnel (LTWT) at Caltech is schematically shown in Fig. 11. Different configurations are of course possible with other water sources. The water, sampled near the water tunnel test section (2), passes through a three-way valve (4) which

4. O'Hern, T. J., "Cavitation in Turbulent Shear Flows" Part II, Ph.D. Thesis, California Institute of Technology (in preparation).

5. "Cavitation Inception in Separated Flows", 1981 by J. Katz, California Institute of Technology, Div. of Eng. & Appl. Sci., Report #183-5, p.193.

operates either the by-pass line (11) or the C.S.M. testing line. The water static pressure is measured by a pressure transducer upstream of the test venturi tube (5). Provisions have been made for the installation of a second pressure transducer (7) downstream of the C.S.M. test section to monitor also the exhaust pressure, if necessary.

During test runs the information on the occurrence of cavitation and the water velocity at the throat of the transparent venturi (6) is obtained from a dual beam back-scattering laser Doppler velocimeter (LDV) system described later. The sampled water is collected in the pressure regulated exhaust vessel (8) and periodically returned to the water tunnel using a small pump (9). The flow is controlled by changing the pressure in the exhaust vessel from 0 to 20 psia with the back pressure regulator (17) connected to the compressed air supply (15) and to a vacuum pump (20). The compressed air line includes the filter (14), the pressure regulator (13) and the pressure gauge (12). The needle valve (16) establishes the slowly rising pressure in the exhaust tank necessary for proper operation of the back-pressure regulator (13). By means of the three way valve (4) the compressed air can also be used to force the water out of the water lines.

Cavitation of a tap water sample initially at atmospheric pressure in a 1 mm diameter venturi tube is shown as an example in the picture of Fig.18. The flow velocity is about 14 m/s.

Optics

The C.S.M. optical set-up consists of a dual beam back-scattering LDV system, whose optical elements are schematically shown in Fig. 12.

The laser beam, generated by a 5 mw He-Ne continuum wave laser (1), goes through a beam displacer (dove prism) (2) and a metal-coated beamsplitter cube (3). The separation of the two outcoming beams can be widely adjusted using the beam displacer to change the transverse position of the beam entering the

beamsplitter. In order to reduce the Doppler frequency of the LDV signal and consequently simplify the processing electronics, the beam separation is then four times reduced by a telescopic relay (4 à 5).

After passing through a slit in the front surface mirror (10), the two beams are corrected in a cylindrical lens relay (6 à 7) for the distortions due to the venturi geometry and are finally focused in the test section of the C.S.M. venturi tube (9) by an aspheric lens (8).

The back-scattered light is collected with maximum possible efficiency by the same aspheric lens of high numerical aperture; then it is once again corrected for cylindrical distortion in the cylindrical lens relay (6 à 7) and mostly reflected by the front surface mirror (10) towards the photomultiplier collimating lens (11). The resulting image of the optical probe volume is spacially filtered by a field stop aperture (12) to reduce the optical background noise and finally reaches the photomultiplier tube (13) where is converted into an electric signal.

The actual C.S.M. optical lay-out is shown in Fig. 13, with the plan view at the top of the picture and the side view at the bottom.

Two I-beams in a T-shaped configuration support both the laser (1) and the base plate, where all the other optical components are installed. The laser mount (2) allows fine positioning and orientation of the laser in both the horizontal and vertical planes. The beam displacer (3) is mounted on a micrometric lateral translation stage (4) for repeatable and accurate control of the separation of the two beams emerging from the beamsplitter (5). The distances between the two lenses of the telescopic relay (6 à 8) and of the cylindrical correction relay (11 à 12) are also adjustable in order to respectively insure perfect parallelism of the emerging beams and optimal compensation of the cylindrical distortion.

The C.S.M. blown-glass venturi is contained in a protective cylindrical shell of cast transparent resin for connection to the hydraulic lines (16 & 19) and easy installation and removal. It is also mounted on a longitudinal translation stage to allow the measurement of the flow velocity along its centerline. In addition, the C.S.M. test section (18) can be finely positioned and oriented in both the horizontal and vertical planes for accurate location at the focal point of the optical system. Pressure taps (17) are located in the water inlet and outlet of the test section.

Finally, the photomultiplier field stop aperture (22) can also be accurately positioned in space for optimal reduction of the optical background noise.

Fig. 16 shows a detailed picture of a 1 mm ID venturi tube. The same tube installed in its mount appears in Fig. 18, where the pressure tap connections on the inlet and outlet lines and the aspheric lens of the focusing and collecting optical assembly are also shown.

Signal Processing

An especially designed C.S.M. signal processor is used for real time collection, temporary storage and further transfer to the computer of the following data obtained from a typical C.S.M. run: the occurrence time of cavitation events; the occurrence time, the duration and the number of zero crossings of valid Doppler bursts, and the corresponding upstream water pressure.

The intensity and the Doppler modulated frequency of the photomultiplier signal are respectively used to monitor the occurrence of cavitation and the flow velocity, while the instantaneous upstream pressure of the water is provided by the output of a pressure transducer.

A simplified block diagram of the C.S.M. signal processing and data acquisition is shown in Fig. 14. After an optional pre-amplification stage, the output of the photomultiplier is filtered for separating the Doppler frequency

and sent to the C.S.M. signal processor, where it is further amplified before entering the control unit.

Here a zero level and two couples of adjustable lower and upper threshold levels are used to reject the noise (signal not exceeding the lower level thresholds) and to recognize the presence of a valid burst as coming from a velocity tracer (signal within the lower and upper level thresholds) or from a cavitation bubble (signal exceeding the upper level thresholds). This information is used to deduce the occurrence time of valid bursts from the run time counter and to increment the cavitation event counter, with adjustable maximum capacity, which provides the stop signal for the conclusion of the run. The same threshold levels are also used by the control logics to reject the spurious zero crossings which may be caused by the presence of high frequency noise and to increment the counters for the measurement of the duration and the number of zero crossings of each valid burst coming from a velocity tracer.

The collected data are temporarily stored in a non-permanent memory and finally transferred to a computer after the conclusion of each run for recording on magnetic disk and further reduction.

The C.S.M. electronic instrumentation is mounted in a standard rack shown in Fig.19. Besides the signal processor itself, it includes the power supply units for the laser and the photomultiplier, the electronic filters, an oscilloscope, the pressure transducer exciter and amplifier, and a digital multimeter.

Fig.20 shows the signal processor installed inside a slide-mounted drawer. It consists of a power supply and a modular bus frame containing three electronic boards. The electrical connections to the photomultiplier, to the pressure transducer and to the computer are mounted both on front panel and the rear side of the bus frame. Also mounted on the front panel are the signal processor's commands and controls: the power switch; the push-buttons for system reset, run start, run stop, data unloading to the computer and the light

indicators for power on, and for the execution of the run and data unloading operations.

Data Acquisition & Reduction

The C.S.M. signal processor is currently connected to a Compaq Plus Desktop personal computer with a total resident memory of 640 K, provided with video screen display and two 5.25" diameter floppy disk drives (see Fig.19). However the data transfer has been designed in such a way that virtually any other microcomputer could alternatively be used.

The data collected during each test run consist of 9 Kbytes which are serially transferred to the computer through a standards RS232 port. They contain in compacted form the information on the occurrence time of cavitation events, the corresponding upstream water pressure, the occurrence time, the duration and the number of zero crossings of the valid Doppler bursts.

Two separate BASIC programs respectively perform the acquisition of the raw data and their reduction.

The data acquisition program simply comprises a machine language subroutine which continuously interrogates the serial input port of the computer and sequentially loads in the resident memory the 9 Kbytes of raw data as soon as they are sent by the C.S.M. signal processor.

The reduction program performs the following operations on the data upon request from the operator: raw data display on the video screen and/or storage in a disk file, reconstruction of the physical data from the raw data, display, plotting, validation, statistical analysis and filtering of the physical data; generation of the final data for nuclei number concentration measurement.

During the reconstruction process five 1K-element arrays of physical data are first retrieved from the original 9 Kbytes of raw data in compact format sent by the signal processor. Each array contains the digital measurements of the above five physical quantities in order of acquisition: the occurrence time

of cavitation events; the occurrence time, the duration and the number of zero crossings of the valid Doppler bursts, and the corresponding upstream water pressure. Next, the computer uses the clock frequencies driving the counters of the signal processor and the pressure transducer calibration data to transform these digital measurements into the corresponding dimensional measurements.

The validated Doppler frequencies are then computed by dividing the number of zero crossings of each valid burst by the corresponding burst duration. To avoid excessive errors in the evaluation of the Doppler frequency, only counts with a preselected minimum number of zero crossings are used.

Since the optical control volume extends across the full width of the venturi throat section, the LDV readings also include data coming from flow regions inside the boundary layers. To isolate the velocity information coming from the potential core as well as to eliminate spurious data from various noise sources, statistical filtering is used, i.e., the readings smaller than the average by more than an adjustable multiple of the standard deviation are rejected. The same filtering technique is also applied to the upstream water pressure data.

The velocity information is deduced from the LDV calibration data and used to compute the pressure at the C.S.M. venturi throat from Bernoulli's equation. Then the flow characteristics of the venturi are used to calculate the number concentration of unstable nuclei for the run and the estimate of its standard error.

The density distribution histogram of observed delay times between cavitation events is computed for comparison with the theoretical probability density distribution deduced from the assumption of Poissonian cavitation process, which corresponds to the absence of interactive effects among cavitation events. Finally, a CHI^2 test of agreement is carried out to generate a synthetic measurement of the accuracy of this assumption.

4. SUMMARY

This concludes the description of the basic tasks. The signal processing of the laser output is seen to be a vital feature of the system. For completeness we include herein in Appendix A a more detailed description of this device and the circuit drawings that have been prepared during the construction of the device.

5. ACKNOWLEDGEMENTS

Graduate students O'Hern and d'Agostino have each contributed heavily in the preparation of this report; the physical construction of the laser component parts was carried out by Elton Daly and Joe Fontana of the Keck Hydraulic Laboratory staff. We are indebted to Sue Berkley and Jan Patterson for preparation of the manuscript.

6. REFERENCES

1. Acosta, A. J., "Cavitation Inception", Final Report on Contract N00014-75-C-0378, Report No. E183.7, March 1985.

Figure Captions

Figure 1. Diagram of sharp-edged plate installed in the Low Turbulence Water Tunnel. The stand-off distance of one inch allows boundary layer fluid to escape underneath the plate avoiding contamination of the flow over the sharp edge.

Figure 2. Simultaneous top and side photographs of free shear layer cavitation (a) Cavitation inception $\sigma_1 = 1.52$, Reynolds number based on upstream velocity and twice step height $= 1.52 \times 10^6$ (b) developed cavitation $\sigma = 0.65$, $Re = 2.2 \times 10^6$.

Figure 3. Schematic diagram of the in-line holographic system set up on the LTWT optical bench.

Figure 4. Photograph of the arrangements for in-line holography of the cavitating shear flow. The sharp-edged plate is visible in the test section of the LTWT. The main power supply and control rack for the laser is not visible in this view.

Figure 5. Diagram of the holographic reconstruction system.

Figure 6. Photograph of the in-line holographic reconstruction system.

Figure 7. Hologram of the sharp-edged bluff body with cavitation at inception. This is a doubly pulsed hologram; in the recirculation region small microbubbles can be seen and the physical displacement between the two pulses is visible. A segment of the streamwise cavitating vortex is visible. The demarcation boundary between the shear layer and recirculation region is visible right from the start of the tip of the plate. This is made possible by the very slight density difference in these flow regions. The flow speed is 7m/s the cavitation index is 0.50 and the test fluid has an air content of 3.3 ppm (molar).

Figure 8. Cavitation inception indices in the free shear layer of the bluff body (from Katz, J., O'Hern, T, "Cavitation in Large Scale Shear Flows" to appear J. Fl. Eng., ASME (same as No.25 Ref.1). Note the sharp dependence on dissolved air content.

Figure 9. Comparison of the data of Fig.8 with earlier work by Kermeen & Parkin (1957), Arndt (1978) (both for disks) and Katz (1981) for blunt-faced cylinders.

Figure 10a. High speed movie sequence showing top view of inception, growth, and collapse of an axial cavity. Flow direction is right to left. Note cavity "fills in" vortex core in frames (iii) to (v). Elapsed time between frames is 2 msec. Exposure time is approximately 200 microseconds.

$V_3 = 9.5 m/s \qquad \sigma = 0.88$

$Re_s = 1.84 \times 10^6 \qquad a = 4.70$ ppm.

Figure 10b High speed movie sequence showing top view of fully developed cavitation in the shear layer. Flow direction is right to left. Growth of axial cavities in braid region between adjacent spanwise vortices is seen between frames (i) and (ii) and between frames (v) and (vi). Elapsed time between frames is 4.2 msec. Exposure time is approximately 170 microseconds.

$V_3 = 11.60 m/s \qquad \sigma = 0.63$

$Re_s = 2.26 \times 10^6 \qquad a = 2.72$ ppm.

Figure 11. C.S.M. set-up schematic (1) Water tunnel (2) Water sampling (from water tunnel) (3) One way valve (4) Three way valve (5) Upstream pressure transducer (6) Transparent venturi tube (7) Downstream pressure transducer (8) Pressure regulated discharge tank (9) Water pump (10) Water return (11) Venturi by-pass line (12) Pressure gauge (13) Back-pressure regulator (14) Air filter (15) Compressed air inlet (16) By-pass needle valve (17) Pressure regulator (18) Vacuum reservoir (19) Water trap (20) Vacuum pump (21) He-Ne laser (22) Beamsplitter (23) Focusing and collecting optics (24) Front surface mirror (with slit for transmission of laser beams) (25) Collimating lens (26) Field stop aperture (27) Photomultiplier

Figure 12. C.S.M. optical components. The beam separation and the cylindrical lens corrector assembly are all adjustable. A dual beam backscatter system is used with a fast aspheric lens (f/=.62) to focus and efficiently collect the scattered light from the venturi. The adjustable beam separation permits operation over a wide flow velocity range with contained Doppler frequency in order to simplify the design of the signal processing electronics. The numbers refer to the components below: (1) He-Ne Laser (2) Beam displacer (dove prism, transversly positionable) (3) Metal coated beamsplitter cube (4) First lens of telescopic relay (5) Second lens of telescopic relay (6) First correcting cylindrical lens (positionable) (7) Second correcting cylindrical lens (8) Focusing and collecting aspheric lens (9) Transparent venturi tube (10) Front surface mirror (with slit for transmission of laser beams) (11) Photomultiplier collimating lens (12) Photomultiplier field stop aperture (positionable) (13) Photomultiplier tube

Figure 13. C.S.M. Machine drawing, top and side views. The scale of the figure is 1:6. The numbers identify the following components: (1) He-Ne laser (2) Laser mount (fully orientable and positionable) (3) Beam displacer (dove prism) (4) Micrometric side translation stage (5) Beamsplitter cube (6) First lens of the telescopic relay (7) Telescopic lens relay (8) Second lens of the telescopic relay (positionable) (9) Front surface mirror (with slit for transmission of the laser beams) (10) Longitudinal translation stage (11) First correcting cylindrical lens (12) Second correcting lens (13) Focusing and collecting aspheric lens (14) Transverse translation stage (15) Venturi tube mount (fully orientable and positionable) (16) Venturi inlet tube (17) Pressure tap (18) Transparent venturi tube (19) Venturi outlet tube (20) Collimating lens (21) Field stop aperture mount (positionable) (22) Field stop aperture (23) Photomultiplier

Figure 14. Block diagram of information flow for the C.S.M. Signal Processor. The threshold levels for noise rejection and Doppler burst validation are adjustable as is the number of bubble counts for test run termination.

Figure 15. General view of the C.S.M. set-up. In the foreground are the I-beams supporting the laser and the baseplate where most of the optical and fluidic components are mounted. In the background are the rack (right) carrying the electronic instrumentation and the data acquisition computer (center).

Figure 16. Close-up view of a C.S.M. venturi tube. A cylindrical shell of cast transparent resin contains the glass-blown venturi tube for mechanical protection, connection to the input and output hydraulic lines and easy installation and removal.

Figure 17. Detailed view of the C.S.M. venturi tube mount. It provides fine positioning and orientation of the venturi in both the horizontal and vertical planes for accurate location at the focal point of the optical system. The longitudinal translation stage allows the measurement of the flow velocity all along the centerline of the venturi.

Figure 18. Cavitation of a tap water sample initially at atmospheric pressure in the 1 mm diameter venturi tube of Fig. 7. The flow velocity is about 14 m/s.

Figure 19. C.S.M. electronic rack. From the top to the bottom: digital multimeter, pressure transducer exciter and amplifier, laser power supply, oscilloscope, electronic filters, C.S.M. signal processor, photomultiplier power supply. On the right the data acquisition and reduction computer: a Desktop Compaq Plus computer with video screen and two 5.25" diameter floppy disk drives.

Figure 20. Close-up view of the C.S.M. signal processor in its slide-mounted drawer. The modular bus frame contains three electronic boards connected to the front panel commands and controls.

TABLE I

Some measured velocity components near one of the streamwise vortex cores. The freestream speed is nominally 7 m/s. Vx is the measured velocity in the direction of flow, Vy is normal (up) and Vz is in the spanwise direction. The cavitation index is about 0.5. The three dimensional nature of the flow is clear from various holograms.

Object	Vx(m/s)	Vy(m/s)	Vz(m/s)
125 μm bubble	-0.44	0.44	-2.55
150 μm bubble	3.46	-1.71	-0.86
85 μm bubble	1.68	-0.13	-0.04
145 X 165 μm sheared bubble	2.70	-2.54	-2.70
90 μm bubble	-0.28	0.10	-0.86
110 μm bubble	-0.82	-0.54	-1.98
80 μm bubble	1.08	-0.36	0.55
90 μm bubble	-0.40	-0.49	0.72
140 μm bubble	1.10	-0.21	0.81
160 μm bubble	0	0.54	1.35
vortex core 230 μm long	1.33	0.83	0.60

TABLE II

Relative strength of streamwise and spanwise vortices

Data pt	U(m/s)	Reynolds No.	Inception Index σ_i	core r_c (in.)	Γ_s (m^2/s)	Γ_p (m^2/s)	Γ_s/Γ_p
1	10.41	2.0×10^6	1.015	.037	.044	.686	.064
2	10.41	2.0×10^6	1.015	.028	.033	.897	.037
3	7.81	1.52×10^6	1.524	.052	.056	.448	.125
4	7.81	1.52×10^6	1.519	.052	.056	.653	.086
5	10.41	2.0×10^6	1.015	.037	.044	.728	.060

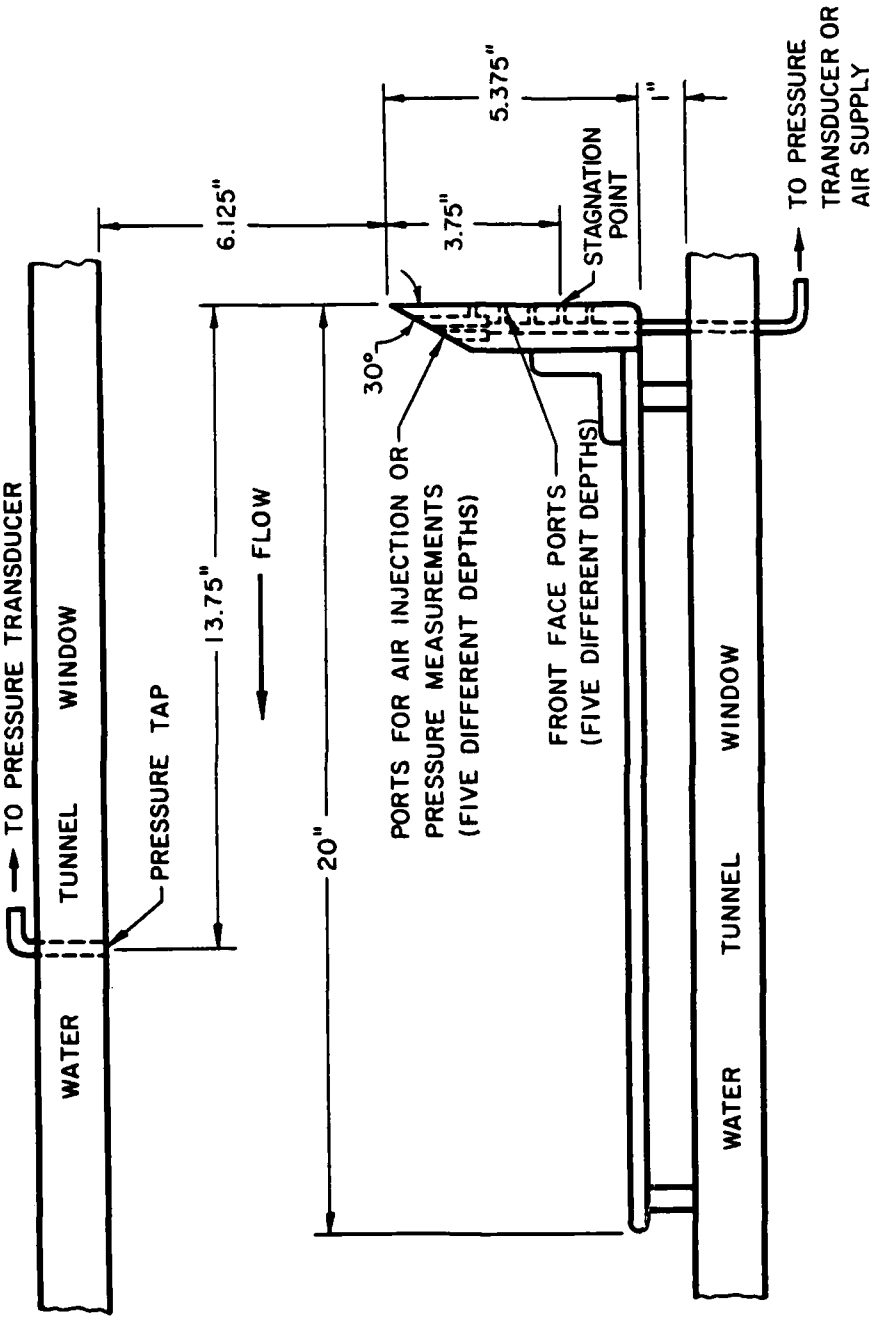
TO PRESSURE TRANSDUCER
TUNNEL WINDOW
PRESSURE TAP
WATER
13.75"
FLOW
20"
6.125"
3.75"
5.375"
1"
30°
PORTS FOR AIR INJECTION OR
PRESSURE MEASUREMENTS
(FIVE DIFFERENT DEPTHS)
FRONT FACE PORTS
(FIVE DIFFERENT DEPTHS)
STAGNATION
POINT
TO PRESSURE
TRANSDUCER OR
AIR SUPPLY
TUNNEL WINDOW
WATER

Figure 1.

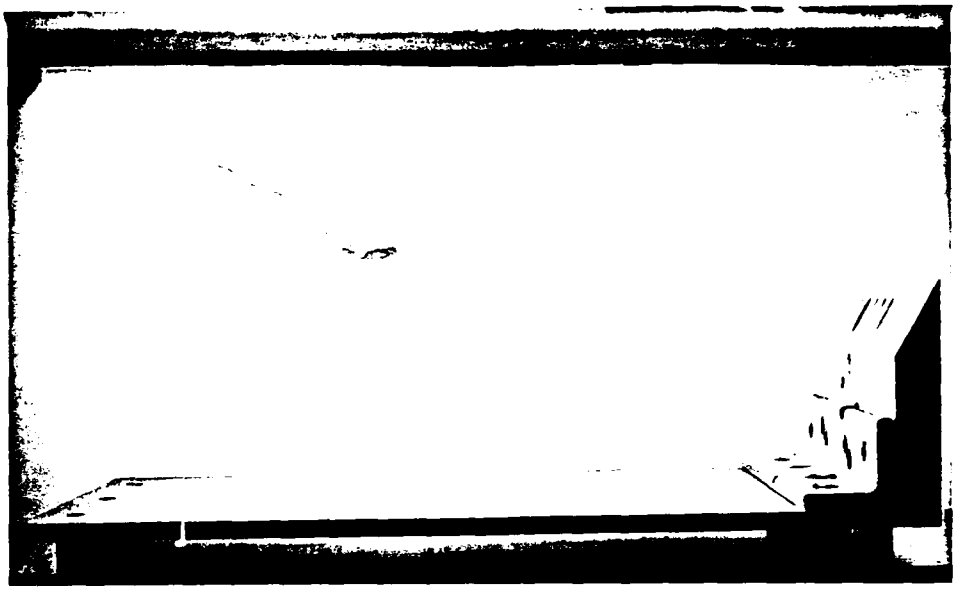

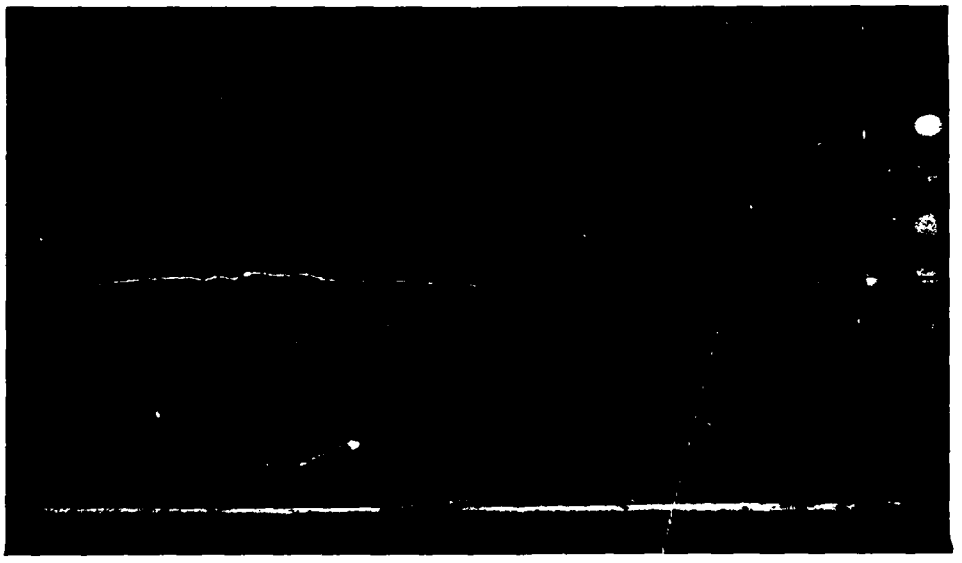

Figure 2a.

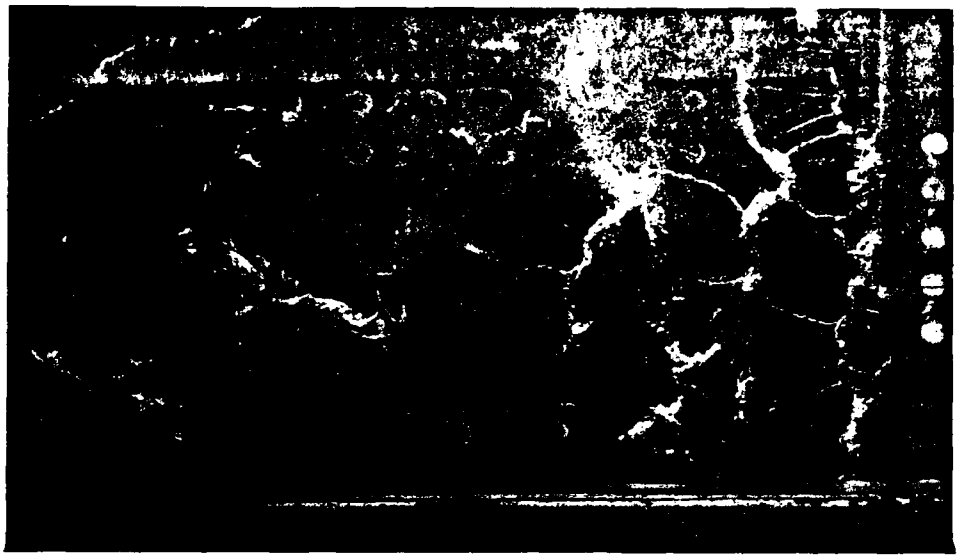

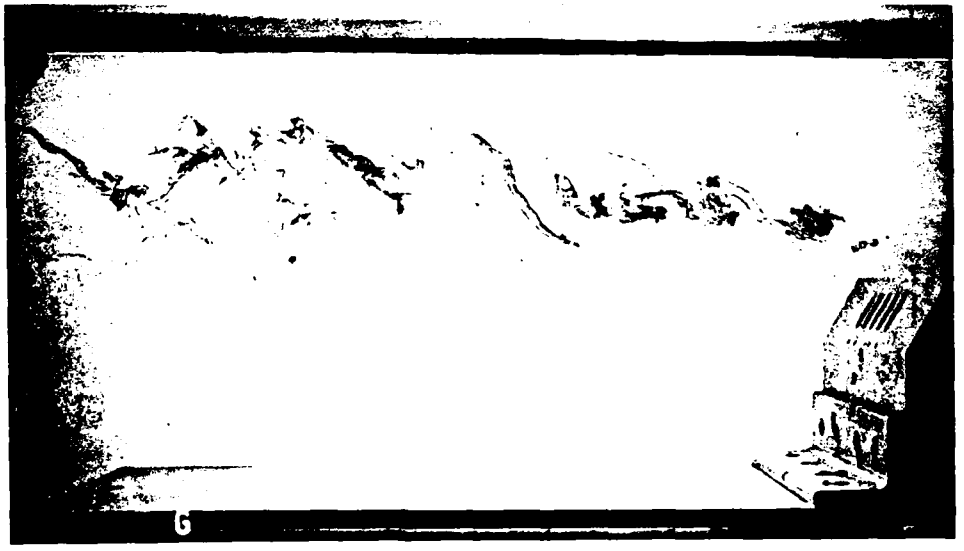

Figure 2b.

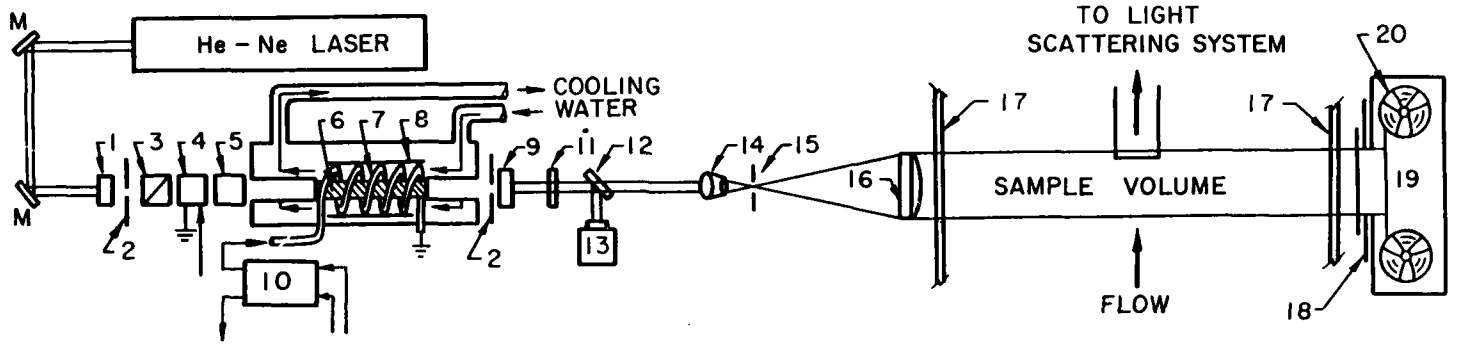

1. BACK MIRROR
2. IRIS APERTURE
3. POLARIZER
4. POCKEL'S CELL
5. POLARIZER
6. RUBY ROD
7. XENON FLASH LAMP
8. REFLECTOR
9. FRONT MIRROR-SAPPHIRE ETALON
10. TRIGGER TRANSFORMER
11. NEUTRAL DENSITY FILTER
12. BEAM SPLITTER (4% REFLECTIVITY)
13. PIN DIODE
M. MIRROR
14. MICROSCOPE OBJECTIVE
15. SPATIAL FILTER-10μ PIN HOLE
16. COLLIMATING LENS
17. GLASS WINDOWS OF THE TUNNEL
18. SHUTTER
19. AUTOMATIC FILM DRIVE
20. HOLOGRAPHIC FILM

Figure 3.

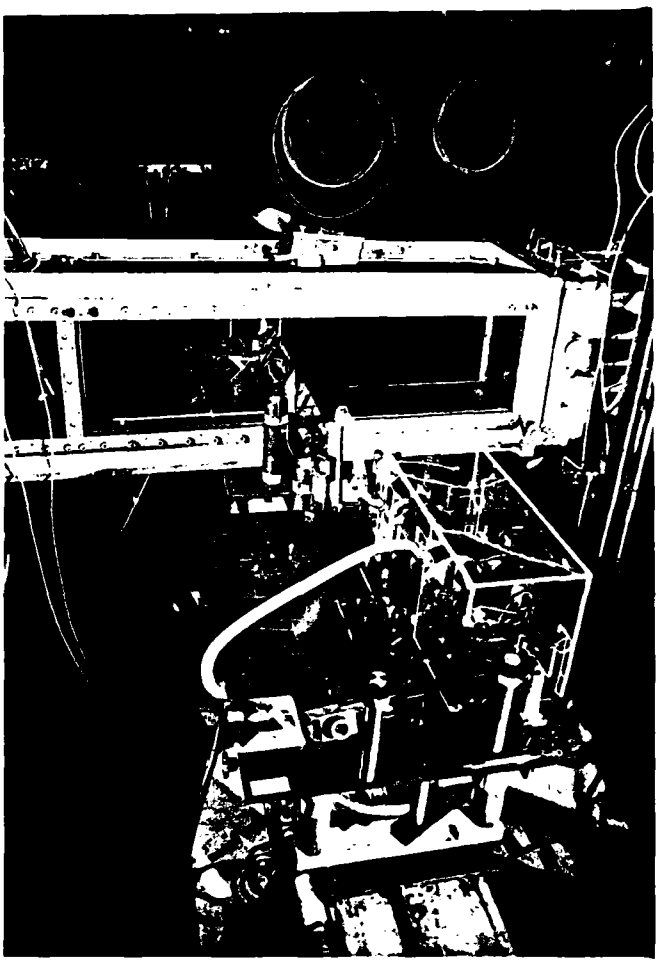

Figure 4.

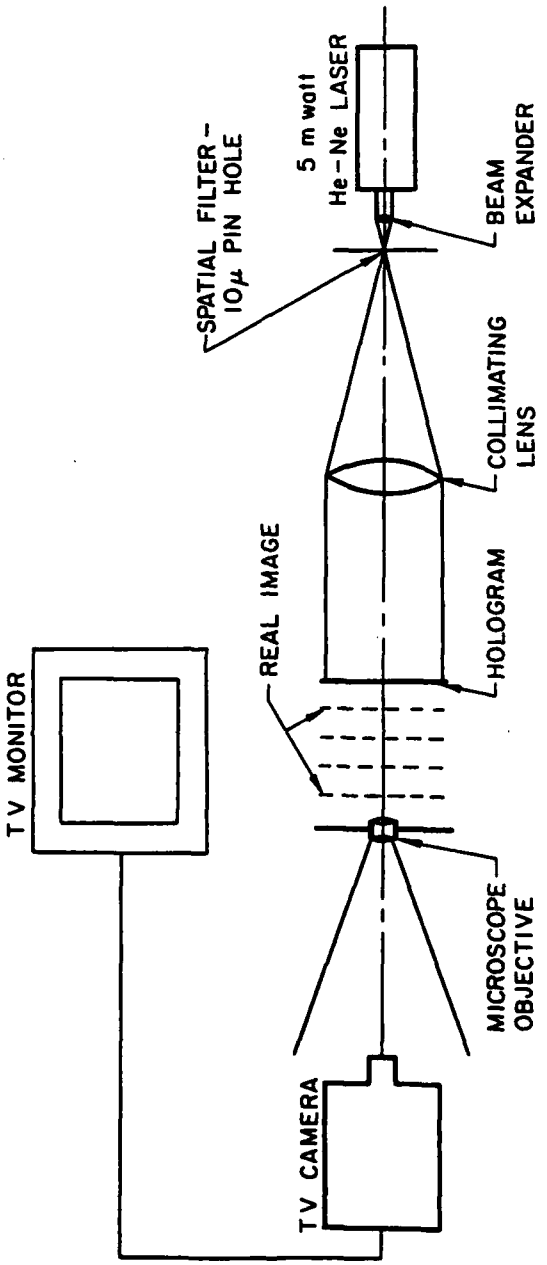
SPATIAL FILTER -
10μ PIN HOLE
5 m watt
He-Ne LASER
BEAM
EXPANDER
COLLIMATING
LENS
HOLOGRAM
REAL IMAGE
TV MONITOR
MICROSCOPE
OBJECTIVE
TV CAMERA

Figure 5.

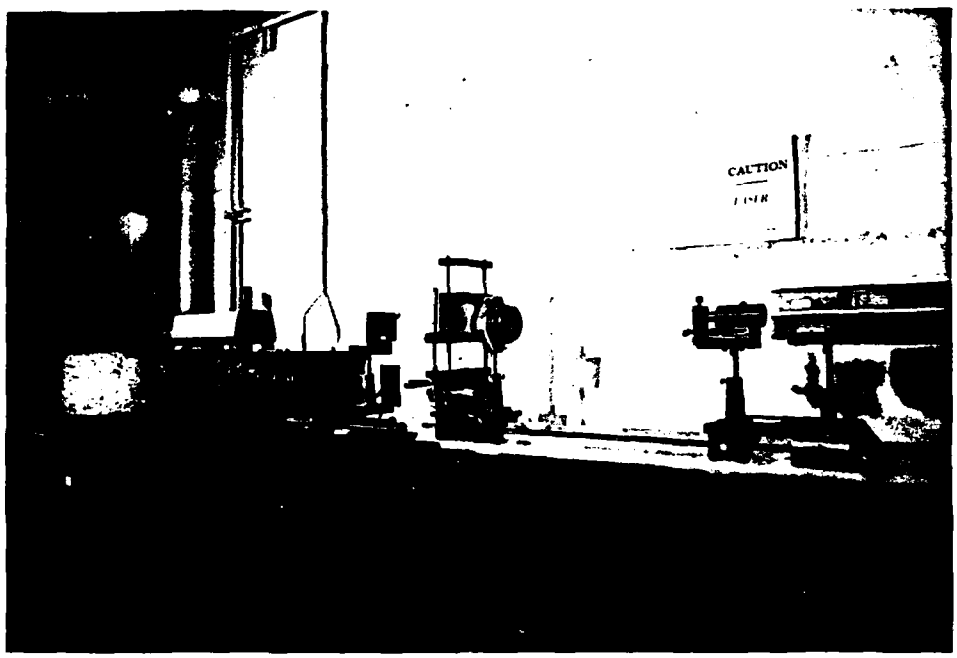

Figure 6.

Figure 7.

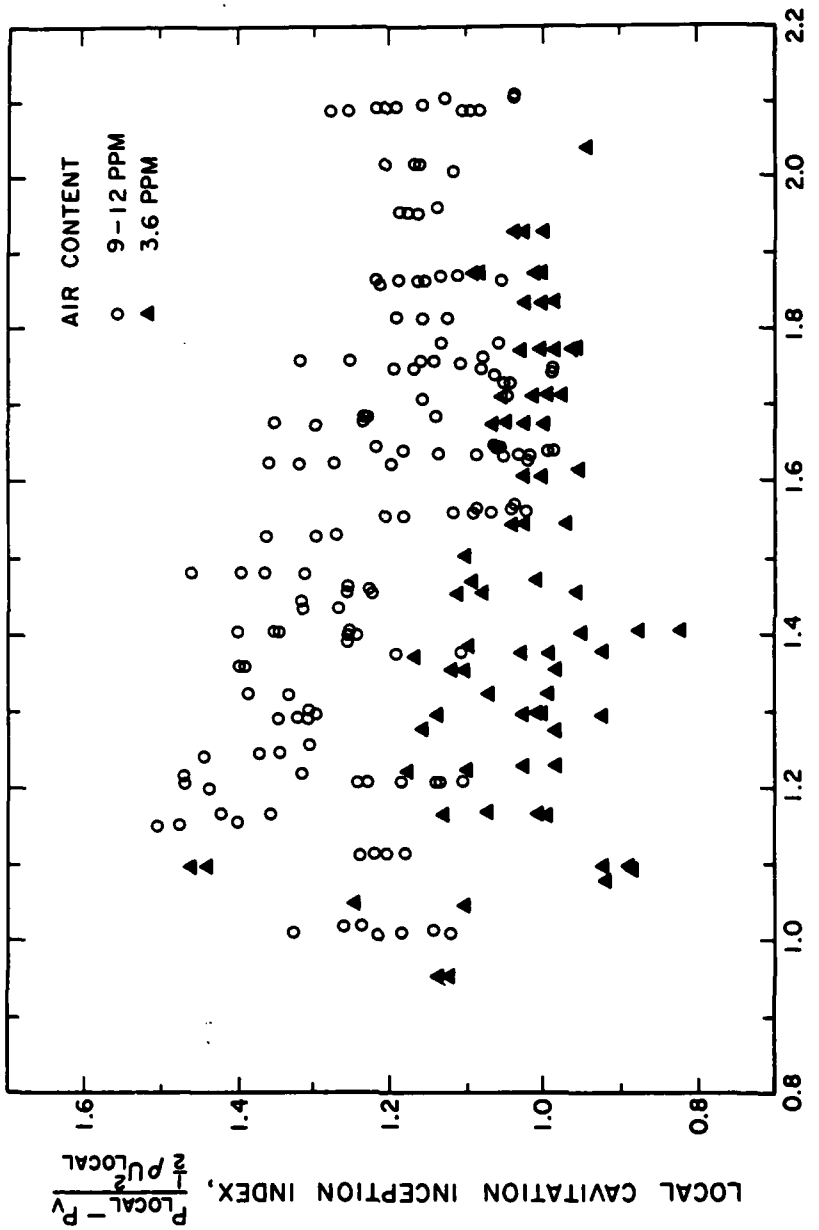
AIR CONTENT
9-12 PPM
3.6 PPM
LOCAL CAVITATION INCEPTION INDEX, $\frac{P_{LOCAL} - P_V}{\frac{1}{2}\rho U^2_{LOCAL}}$
LOCAL REYNOLDS NUMBER, $\frac{U_{LOCAL} \cdot (2S)}{\nu} \times 10^{-6}$
0.8
1.0
1.2
1.4
1.6
1.8
2.0
2.2

Figure 8.

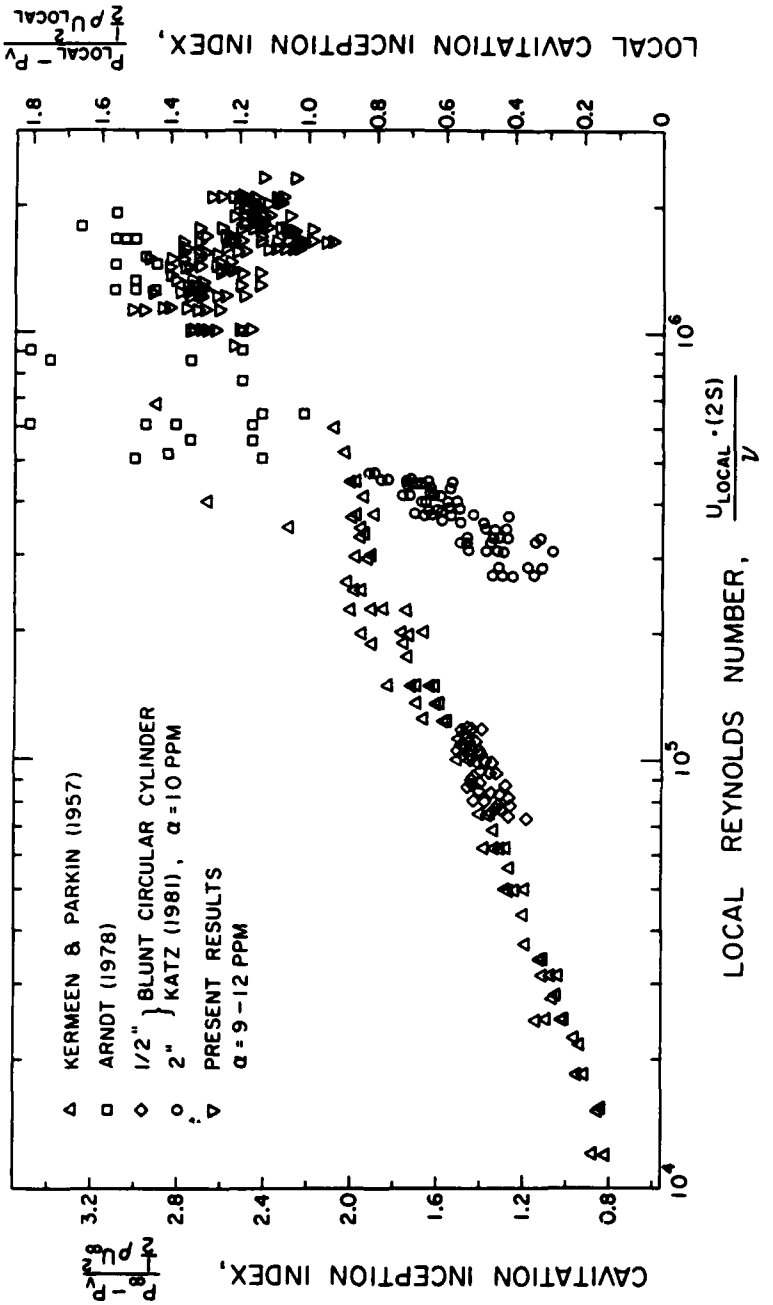
LOCAL CAVITATION INCEPTION INDEX, $\frac{P_{LOCAL} - P_V}{\frac{1}{2}\rho U^2_{LOCAL}}$
CAVITATION INCEPTION INDEX, $\frac{P_\infty - P_V}{\frac{1}{2}\rho U^2_\infty}$
LOCAL REYNOLDS NUMBER, $\frac{U_{LOCAL} \cdot (2S)}{\nu}$
KERMEEN & PARKIN (1957)
ARNDT (1978)
1/2" } BLUNT CIRCULAR CYLINDER
2" } KATZ (1981), α = 10 PPM
PRESENT RESULTS
α = 9 - 12 PPM

Figure 9.

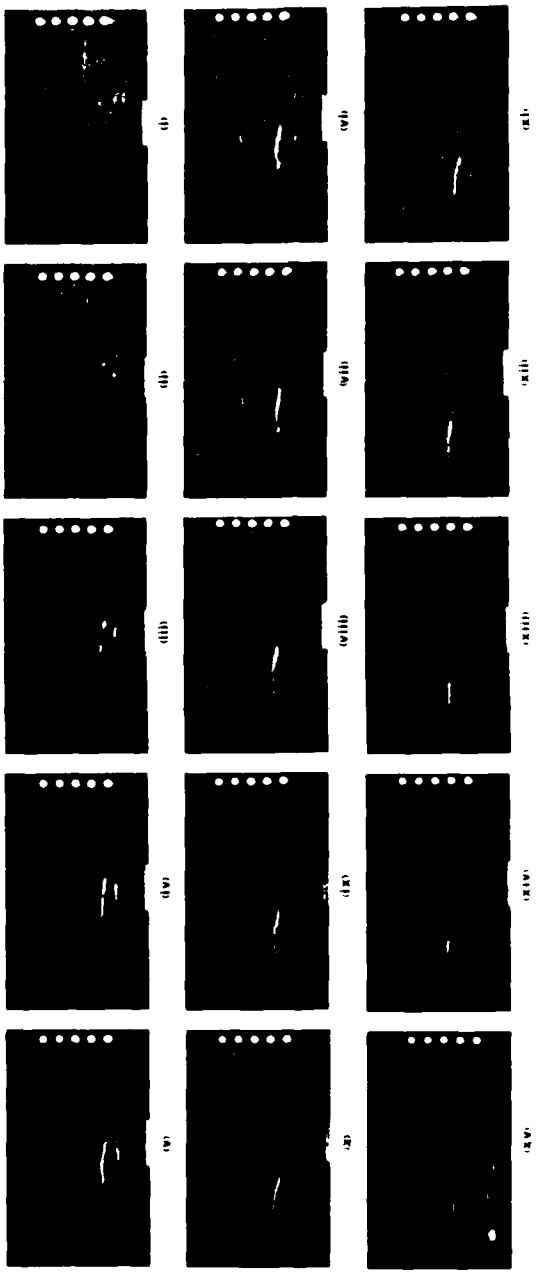

Figure 10a.

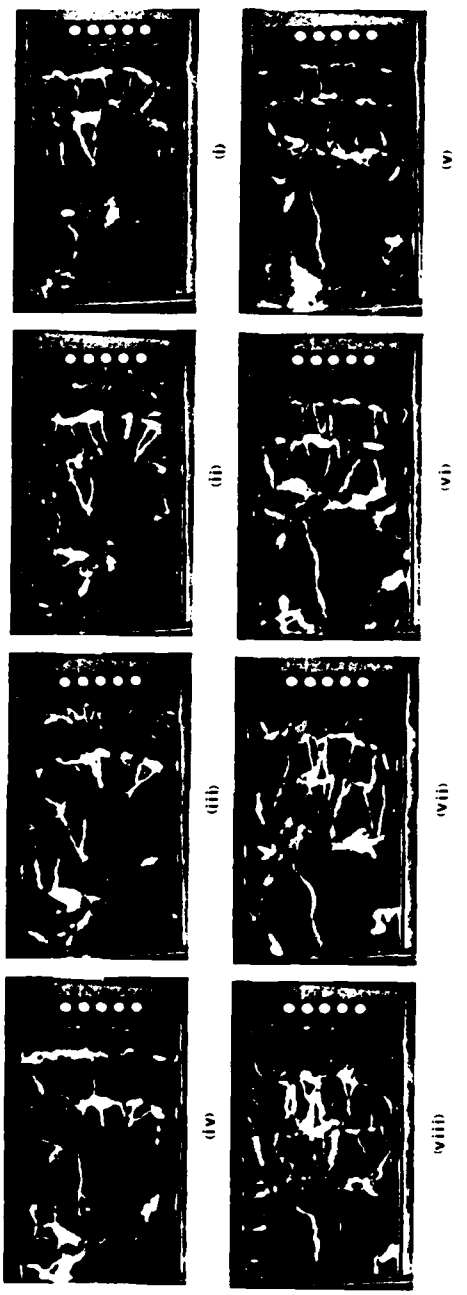

Figure 10b.

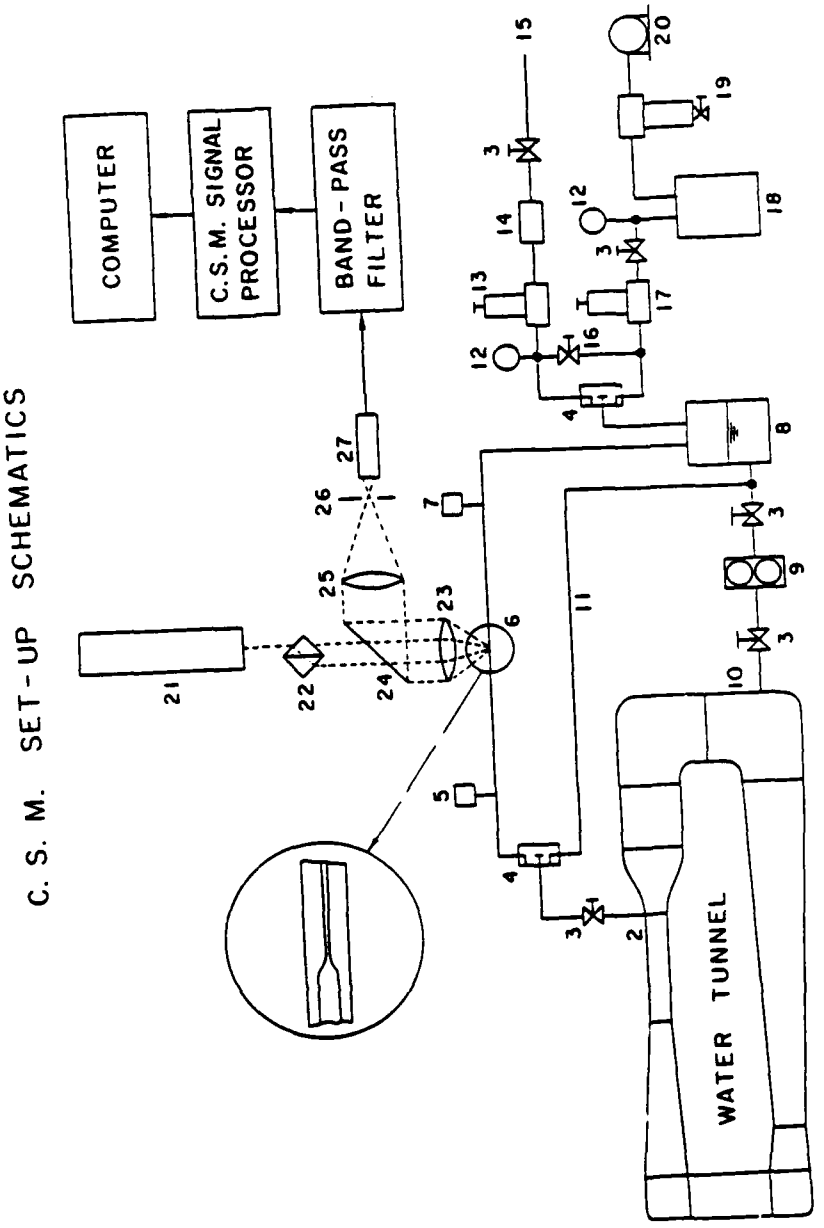
C. S. M. SET-UP SCHEMATICS
COMPUTER
C.S.M. SIGNAL PROCESSOR
BAND-PASS FILTER
WATER TUNNEL

Figure 11.

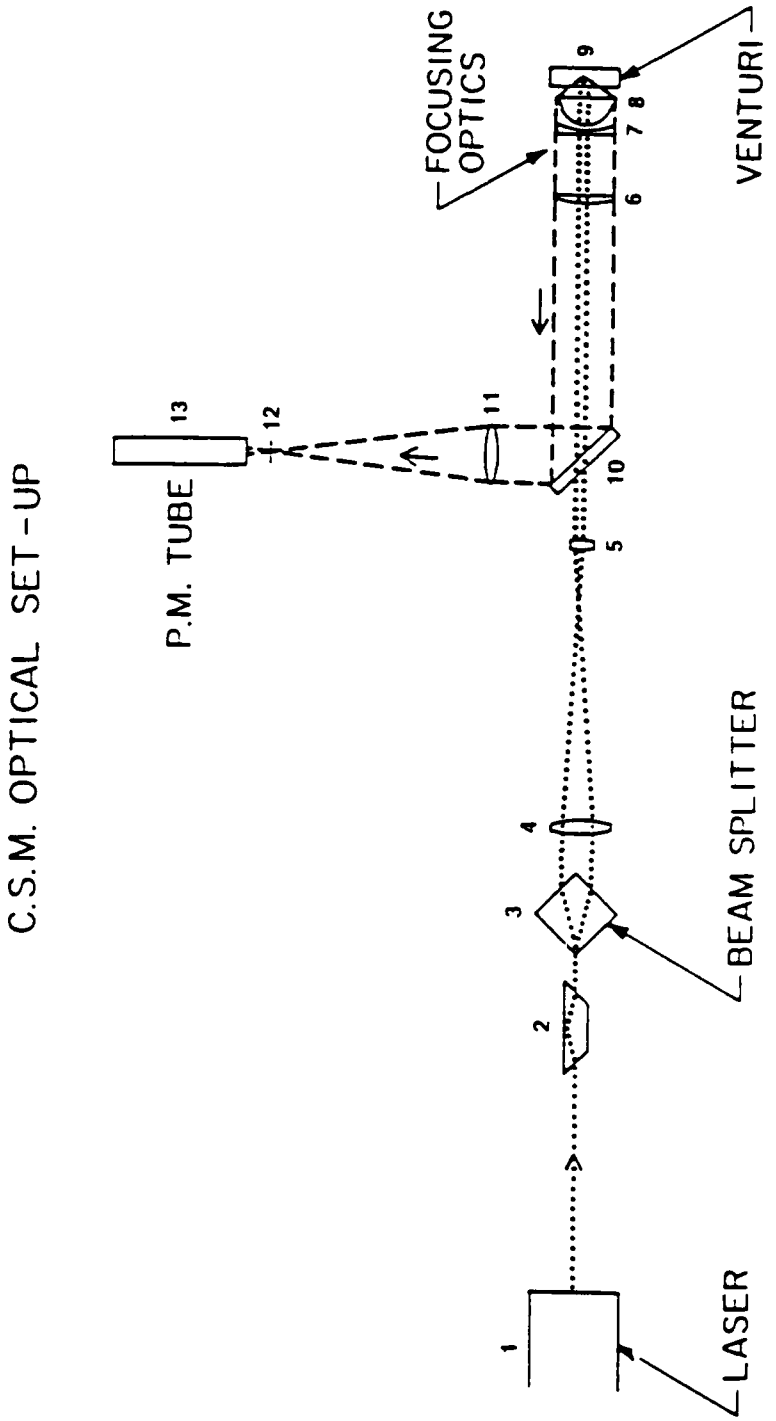
C.S.M. OPTICAL SET-UP
P.M. TUBE
FOCUSING OPTICS
VENTURI
BEAM SPLITTER
LASER
1
2
3
4
5
6
7
8
9
10
11
12
13

Figure 12.

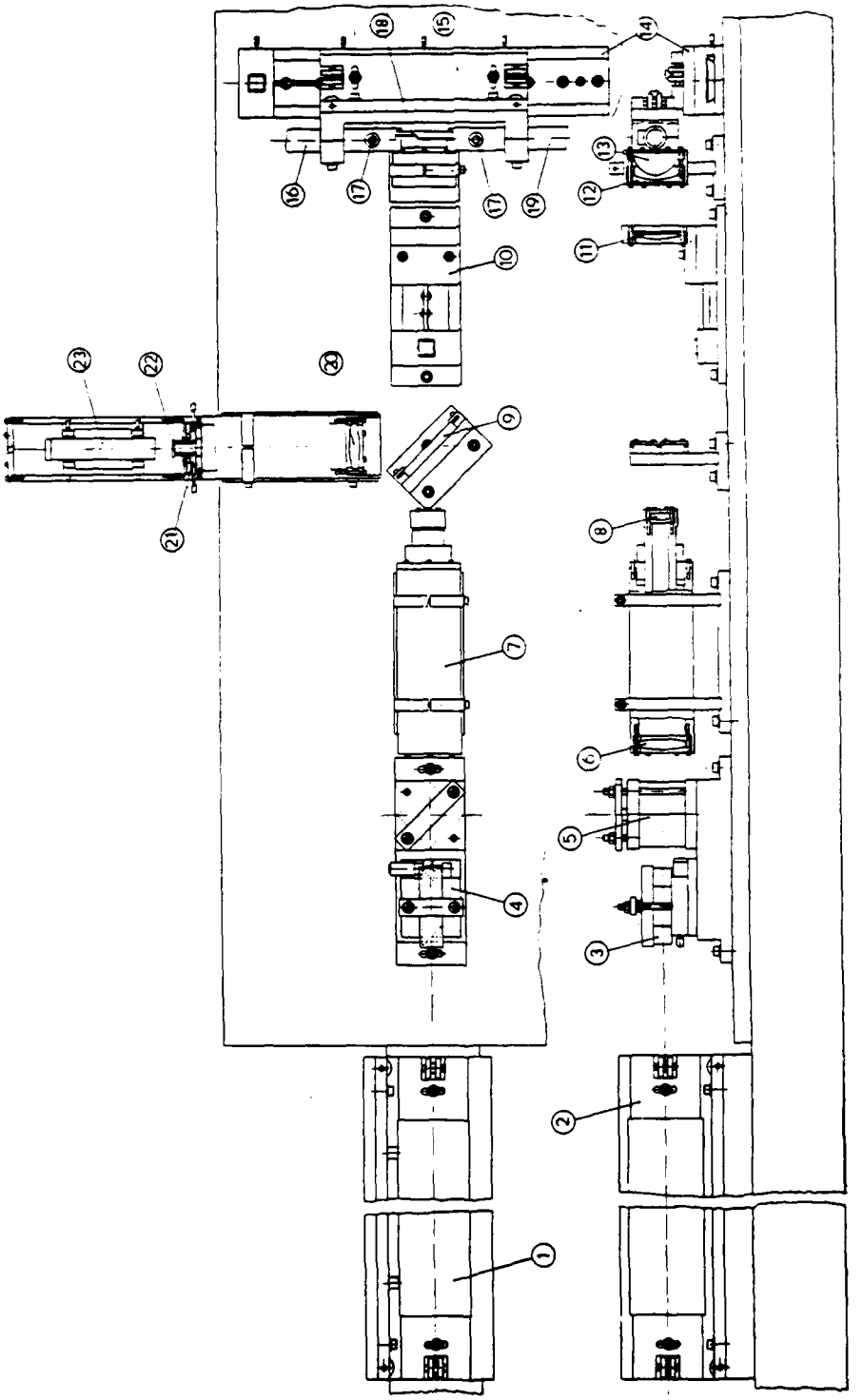

Figure 13.

BLOCK DIAGRAM OF C. S. M. INFORMATION FLOW

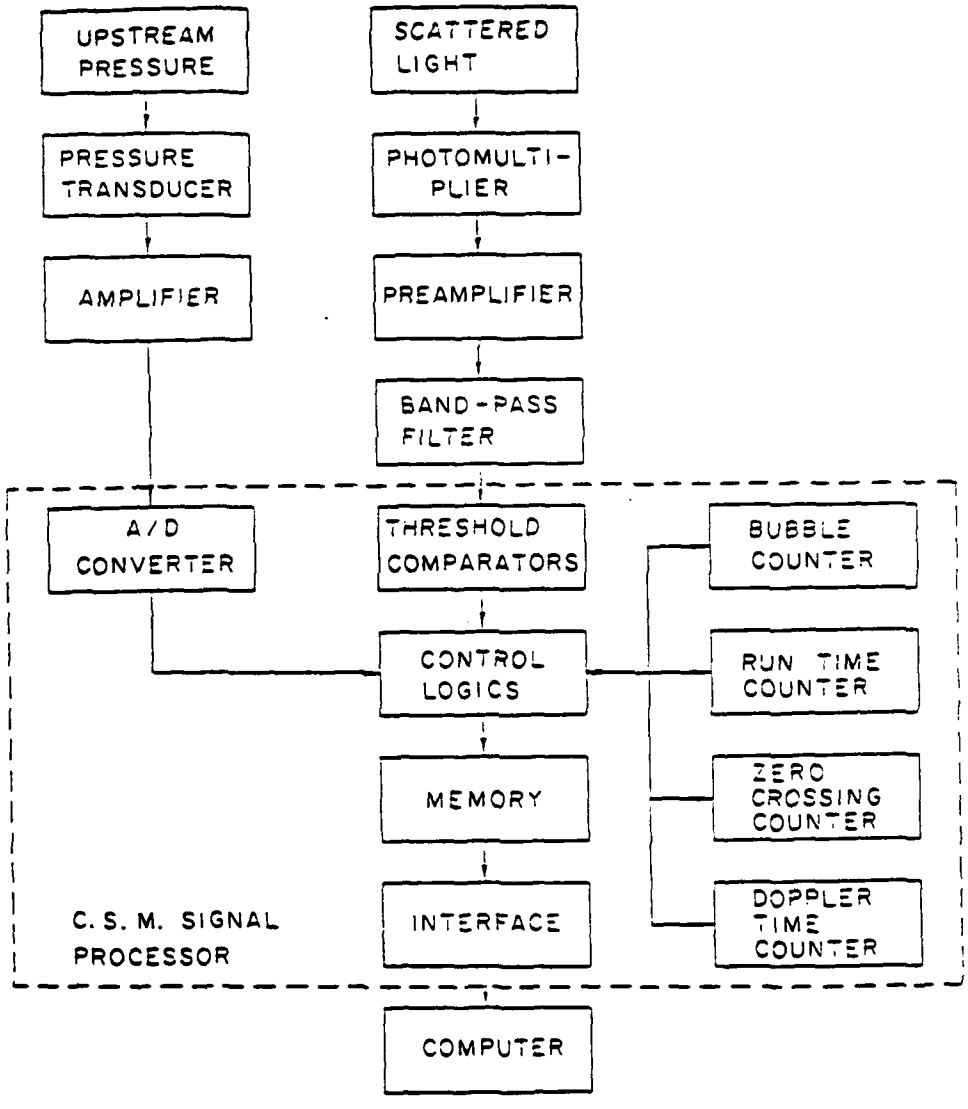

Figure 14.

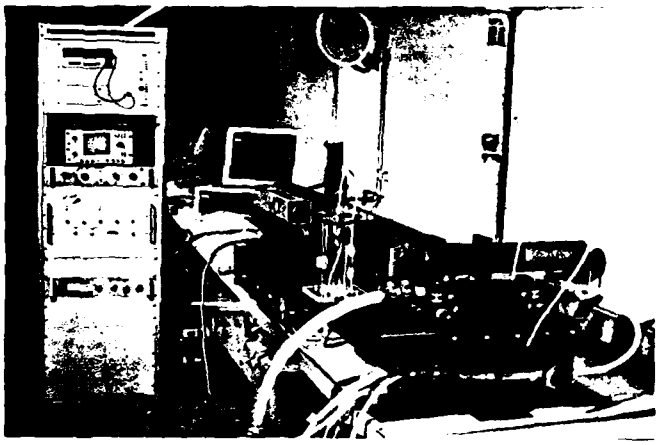

Figure 15.

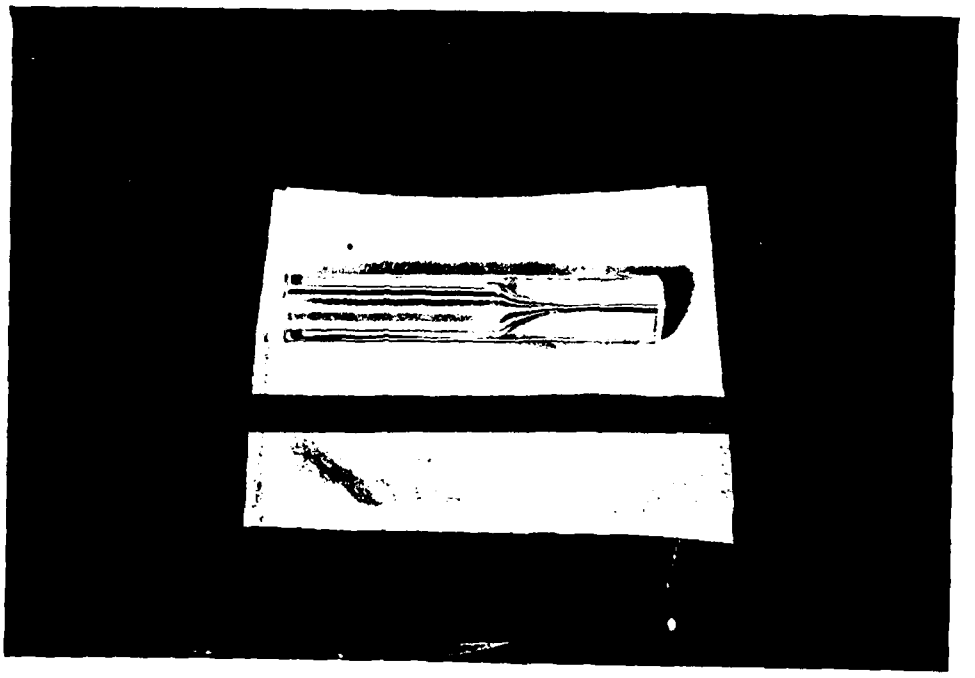

Figure 16.

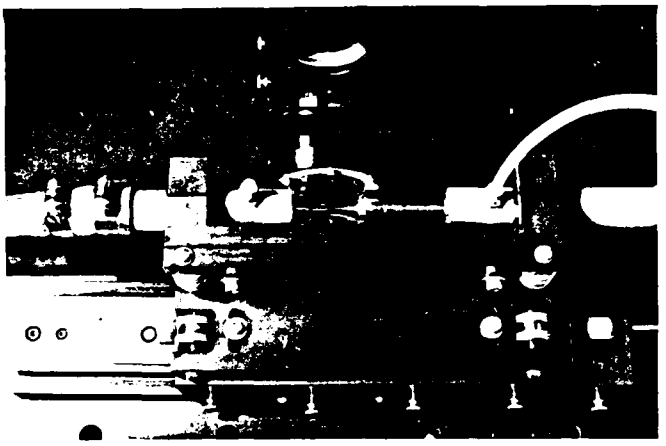

Figure 17.

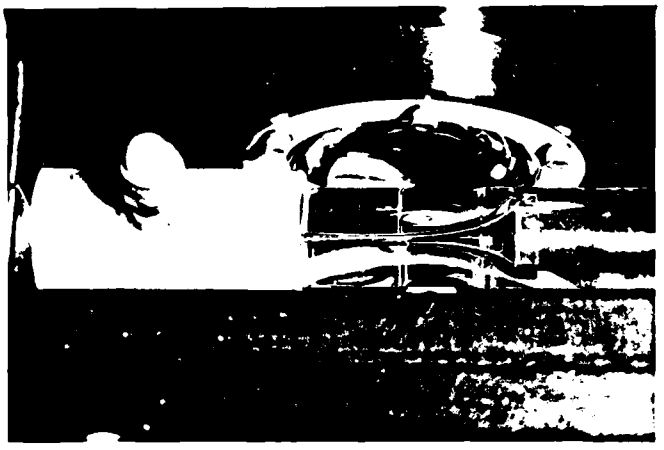

Figure 18.

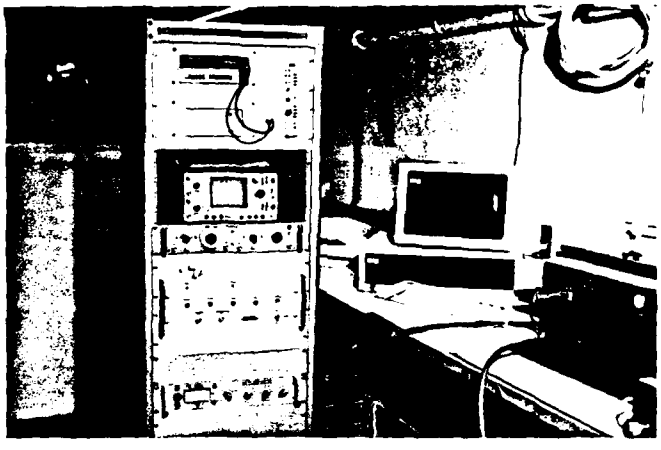

Figure 19.

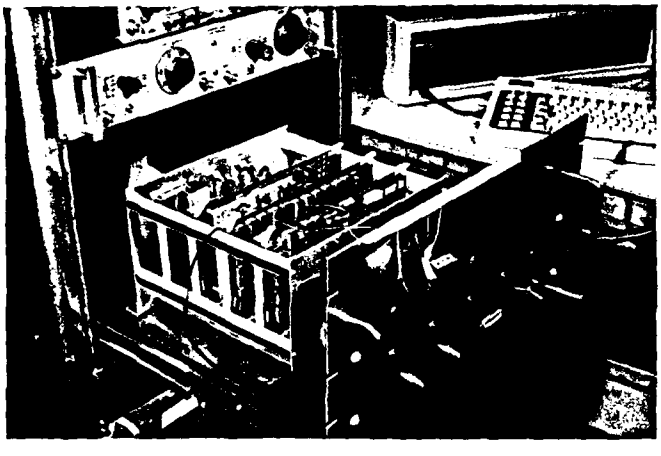

Figure 20.

Appendix A

The Signal Processing Unit

THE LDV SIGNAL PROCESSOR*

1. Generalities

The LDV signal processor is used for real time collection, temporary storage and further transfer to the computer of the following data obtained from a typical C.S.M. run: the occurrence time of cavitation events or bubbles, the upstream pressure and the occurrence time, duration and number of zero crossings of valid Doppler bursts or particles.

The intensity and the Doppler modulated frequency of the photomultiplier signal are respectively used to monitor the occurrence of cavitation and the flow velocity, while the instantaneous upstream pressure of the water is provided by the output of a pressure transducer.

A simplified block diagram of the C.S.M. signal processing and data acquisition is shown in Fig. 1. After an optional pre-amplification stage, the output of the photomultiplier is filtered for separating the Doppler frequency and sent to the C.S.M. signal processor, where it is further amplified before entering the control unit.

Here a zero level and two symmetric adjustable lower and upper threshold levels are used to reject the noise (signal not exceeding the lower level thresholds) and to recognize the presence of a valid burst as coming from a velocity tracer or particle (signal within the lower and upper level thresholds) or from a cavitation event or bubble (signal exceeding the upper level thresholds). This information is used to deduce the occurrence time of valid bursts from the run's Elapsed Time Counter (ETC) and to increment the cavitation event counter (Bubble Address Counter, BAC), with adjustable maximum capacity, which provides the stop signal for the conclusion of the run. The same threshold levels are also used in proper sequence by the control logic to reject the spurious zero crossing which

* Prepared by Luca d'Agostino

may be caused by the presence of high frequency noise and to operate the counters for the measurement of the duration (Particle Duration Counter, PDC) and the number of zero crossings (Zero Crossing Counter, ZCC) of each valid burst coming from a velocity tracer.

The collected data are temporarily stored in a non-permanent memory and finally transferred in serial form to a computer after the conclusion of each run for recording on magnetic disk and further reduction.

The LDV signal processor is installed inside a slide mounted drawer in a standard relay rack together with the rest of the C.S.M. electronic instrumentation. It consists of a modular bus frame containing three electronic boards, a power supply and the commands, controls and input/output electrical connections to the LDV photomultiplier, the pressure transducer and the computer.

2. Drawing List

1 Control Stuff

2 Particle Duration Counter

3 Bubble Count Comparator

4 Dividers

5 Particle Sample Time

6 Memory and Buffers

7 Memory and Buffers

8 Elapsed Time Counter

9 Zero Crossing Counter

10 RS232 Data Interface

11 Threshold Circuits

12 LDV Amplifier

13 More Memory Stuff

14 Analog to Digital Converter

15 Power Supply Capacitors for Boards 1, 2 & 3

16 LDV Comparators

17 Chassis Wiring Diagram

18 Board Interconnect 1

19 Board Interconnect 2

20 Board 1 Lay-out

21 Board 2 Lay-out

22 Board 3 Lay-out

3. Nomenclature

The electronic boards are identified by their number, which is also written on each of them. The individual electronic components of the C.S.M. signal processor are indicated with the symbols used in the relevant drawings. Thus, for example:

U23A-3	identifies pin 3 of the unit No. 23A
TP15	identifies test point No. 15 (and the corresponding signal)
R60	identifies resistor No. 60
C12	identifies capacitor No. 12
[78]	identifies point No. 78 (and the corresponding signal)
Q7	identifies transistor No. 7

Furthermore, the main subsystems are indicated as follows:

ETC: Elapsed Time Counter, counts time from the beginning of the run

PDC: Particle Duration Counter, counts duration of velocity tracers

ZCC: Zero Crossing Counter, counts zero crossing of velocity tracers

BAC: Bubble Address Counter, counts memory address of cavitation event data

PAC: Particle Address Counter, counts memory address of particle data

Additional notations for commonly occurring signals are:

EPS: Enable Particle Stuff signal, gates particle sampling from LDV signal

GT: particle Gate Time signal

ZC: Zero Crossing pulse train signal

A: memory reset at run start

RUN: run under way

UL: data unloading under way

Inh: bubble occurrence

RST: system reset

4. Functional Description of Main Circuits

The following brief description is intended to provide an introduction to the concepts of the C.S.M. signal processor operation and a general overview of its most important components. Since from the user's point of view it is mostly important to understand the meaning and possible limitations of the collected information, more emphasis is given on the way data are generated than on the way they are handled by the control logic. The various circuits are introduced and discussed in the order that made the functional description of the entire system easier to follow.

LDV Amplifiers

Sheet 12 - Board 3

The LDV signal from the photomultiplier tube, after optional external pre-amplification, enters the board through TP13 and goes to a first medium gain amplifier (transistors Q1, Q3, Q4) which in turn drives in parallel a high gain amplifier (transistors Q5, Q6) with output at TP14 for particle detection and a low gain amplifier (transistors Q8, Q9) with output at TP15 for bubble detection.

LDV Comparators

Sheet 16 - Board 3

The outputs TP14 and TP15 of the LDV signal amplifiers go to the comparators:

U25 positive bubble threshold

U26 positive particle threshold

U27 zero crossing particle threshold

U28 negative particle threshold

U29 negative bubble threshold

For proper noise rejection and bubble/particle discrimination each couple of thresholds must be set precisely symmetric with respect to the zero level. The variable resistors for adjusting the comparator thresholds are located close to the top edge of the board. From right to left they are:

R60 for TP3, positive bubble threshold

R63 for TP4, positive particle threshold

R66 for TP5, zero crossing threshold

R69 for TP6, negative particle threshold

R72 for TP7, negative bubble threshold

The comparators generate the following digital outputs with feed-back signals:

U26 with output at TP9 and feed-back at TP17

U27 with output at TP10 and no feed-back

U28 with output at TP11 and feed-back at TP18

U25 with output at TP8 and feed-back at TP16

U29 with output at TP12 and feed-back at TP19

for the threshold circuits (sheet 11).

Threshold Circuits

Sheet 11 - Board 3

The threshold circuits operate on the output of the LDV comparators to generate the following signals for the control stuff:

[33] validated bubble signal

[32] bubble Doppler fringe signal

[31] particle gate time signal

[72] particle zero crossing pulse train signal

[78] enable particle stuff signal

The output TP10 of the zero crossing comparator U27 goes to the system of units U34, U35A, U36A, U36B, U94A which respectively generate a short pulse in response to: a negative zero crossing (U36B-4), a positive zero crossing (U94A-3) or to any zero crossing either positive or negative (U35A-3).

The flip-flops U30A (positive bubble threshold), U31A (positive particle threshold), U31B (negative particle threshold) and U95A (negative bubble threshold) receive their clock signals TP8, TP9, TP11, TP12 from the corresponding threshold comparators U25, U26, U28, U29 and their reset signals form the zero crossing pulse generators of opposite sign. Thus their outputs reflect the presence of LDV signal from bubbles or particles which has exceeded the corresponding positive or negative thresholds but has not yet reached zero.

The signals from the positive and negative bubble threshold flip-flops U30A-5 and U95A-5 are then logically added in U35B, whose output [33] therefore reflects the presence of LDV signal which has exceeded either the positive or negative bubble threshold but that has not yet reached zero. This signal indicates the occurrence of a Doppler fringe from a cavitation event or bubble.

The main signals generated by the bubble threshold circuits are shown in Fig.2.

In the same way, the signals from the positive and negative particle threshold flip-flops U31A and U31B are logically added in U35C, whose output thus reflects the presence of LDV signal which has exceeded either the positive or negative particle threshold but that has not yet reached zero. This signal indicates the occurrence of a Doppler fringe from a velocity tracer or particle.

The unit U30B uses the signals from U35B (bubble Doppler fringe signal) and from the zero crossing pulse generator U35A to produce a short pulse to reset the counter U33 only when a bubble fringe is not present at the time of a zero crossing. The delayed feed-back from pin 9 to pin 10 through R74 and C41 is used to adjust the duration of the pulse.

The unit U33 counts the positive transitions of the bubble Doppler fringe signal from U35B until it is stopped by the feed-back 13 when the maximum count number set by the jump S5 is reached. The unit is reset by the signal from U30B, i.e. by the first zero crossing occurring when no bubble Doppler fringe is present. The signal [33] is therefore used for bubble signal validation.

The unit U32A generates two complementary signals TP17 and TP18 [31] whose value is determined by the value of the particle Doppler fringe signal (input 2) from U35C at the time of a zero crossing as indicated by the clock input 3 from the zero crossing pulse generator U35A. The unit is reset by the signal [78] (Enable Particle Stuff). Therefore its output [31] is the particle gate time signal.

The unit U32B generates short pulses set by the presence of particle Doppler fringe signal from U35C at the time of a zero crossing from U35A (zero crossing pulse generator) and reset by the time delayed feed-back (pin 8 and 13) if signal [78] (enable particle stuff) is present. The resulting signal [72] is therefore the particle zero crossing pulse train. The main signals generated by the particle threshold circuits are shown in Fig. 3.

Control Stuff

Sheet 1 - Board 1

The Control Stuff activates and synchronizes the components of the LDV signal processor in response to the external commands from the operator and to the internal status of the system in order to perform operations such as: reset, run start and data unload sequences, pressure data A/D conversion, memory data address incrementation, data writing to the memory and run termination.

The following system status signals and their complements are generated and used by the Control Stuff to pilot other components of the signal processor:

[71] or A memory reset at run start

[54] or RUN run under way

[98] or UL data unloading under way

[46] or Inh bubble occurrence

The flip-flop U114A is triggered by the run start command to generate the signal [71] and its complement (pin 2) for memory clearing at the beginning of each run and for control of other components. At the conclusion of the memory reset the second flip-flop U2A generates the signal [54] and its complement (pin 1) indicating that a run is under way until it is terminated by overtime [47], stop command [64], bubble count conclusion from U22-13, power-on reset from U9A, reset command [65] or unload signal [98] from U13B-13.

The unit U13A responds to the unload command [66] generating the start load reset signal [50] and synchronizing the unload flip-flop U13B with the unload clock frequency [99] to produce the signal [98] and its complement [53], which indicate that the data unloading to the computer is under way.

The units U3A, U3B and U4 use the validated bubble signal [33], the 1MHz and 20 kHz clock frequencies to generate the bubble time write enable signal

[29] for the memory and the clock signal (pin 7) for the Bubble Address Counter (BAC), U12.

The unit U21A responds to the bubble fringe signal [32] generating the signal [46] and its complement (pin 2), which therefore indicate the presence (or the absence) of a bubble. They are used to carry out the sequence of operations corresponding to either bubbles or particles by selectively enabling or disabling the proper components of the processor.

The units U115, U21B and U22A use the particle gate time signal [31] and the 2 MHz clock frequency from U82-1 to produce the synchronized clock enable signal (pin 1). Units U23 uses this signal together with the 2 MHz clock frequency to generate the the particle time write enable signal [30] for the memory when pressure data conversion has taken place (signal from U108). Similarly, unit U23 uses the same signal to generate the pressure data write enable signal [49] for the memory and the clock signal (pin Q6) for the Particle Address Counter (PAC), U16.

The unit U17 is activated during the reset or unload sequences and generates the control signals [1] through [8], [56], [57] for sequentially enabling of the output buffers. Finally, the output pulse of unit U2B-13 resets the unload sequences at the end of each data unloading to the computer.

A/D Converter

Sheet 14 - Board 1

The A/D Converter U108 digitizes the analog signal [83] from the pressure transducer.

The input scaling of the A/D Converter can be adjusted to the input signal range by establishing proper connections among the pis 22, 23, 24, 25, 26 and 29. The variable resistor R4 is used for zeroing the unit and the input from U110-2 or U23-2 for initiating the conversion. The buffers U112 and U113

interface the A/D converter output with the pressure data bus and are gated by the signal [71] (memory clearing at run start).

Dividers

Sheet 4 - Board 1

The dividers are used to generate the clock signals of different frequencies needed for the operation and synchronization of the LDV Signal Processor.

The first divider comprises units U82, U83 and U100A connected to the 20 MHz oscillator and produces the following outputs:

U82-11 at 4 MHz, not used

U82-12 at 2 MHz, for particle time writing synchronization

U100-1 at 1 MHz, for bubble time writing synchronization

U83-6 at 200 kHz for particle sample time circuits

[70] at 20 kHz for elapsed time measurement (to ETC)

The output from the 20 MHz oscillator is also directly used by the Particle Duration Counter (PDC) for the measurement of the particle gate time.

The second divider, unit U99, is connected to the 1.8432 MHz oscillator and generates the proper frequency for data output to the RS232C serial port at 9600 baud.

Zero Crossing Counter (ZCC)

Sheet 9 - Board 2

The Zero Crossing Counter U67 is activated by the logical addition of the signal [72] (particle zero crossing pulse train) and [31] (particle gate time). The unit is also reset through pin 11 by any of the following signals:

[46] bubble occurrence

[33] validated bubble signal

[71] memory clearing at run start

[81] reset after writing particle data

Elapsed Time Counter (ETC)

Sheet 8 - Board 2

The Elapsed Time Counter measures the time from the beginning of the run. The counters U68 and U69 are incremented by the signal [70] from the 20 kHz clock U83-14 and are reset by either the signal [54] (run not under way) or [71] (memory clearing at run start). The full 24 bits output is used to record the time of occurrence of cavitation events (bubbles). However, only the 12 most significant bits are used for recording the time of occurrence of velocity tracers (particles), whose resolution is therefore reduced by a factor of 2^{12}. The most significant bit signal [47] is also used to terminate the run when the counter has been used to full capacity (run overtime).

Particle Duration Counter (PDC)

Sheet 2 - Board 1

The Particle Duration Counter measures the time duration of LDV signals from velocity tracers or particles. The counter U70 is incremented by the 20 MHz clock signal only during the particle gate time interval indicated by the signal from U32-2 and it is reset by any of the following signals:

U21-1 bubble occurrence

U6-9 system reset signal

U11-6 reset after writing data to the memory

[71] memory clearing at run start

Bubble Count Comparator

Sheet 3 - Board 1

The Bubble Count Comparator generates the signal for run termination when a preset number of bubbles has been counted.

The chained comparators U72, U73, U74 are connected with the Bubble Address Counter (BAC) and with the multiple switch S1, where the maximum number of bubbles to be counted is coded in binary form by properly setting its 10 individual switches. The output 13 of U72 carries the information whether or not the preset number of bubbles has been reached. The flip-flop U22, with the connections to U111-10, to U114-1 (memory clearing signal run start) and the delayed feed-back between pin 13 and 10, is used to transform the output of the comparator into a brief pulse signal to unit U8-2 of the Control Stuff for run termination.

Particle Sample Time Sheet 5 - Board 1

The Particle Sample Time circuits are used to generate the Enable Particle Stuff (EPS) signal [78] which gates the sampling of particles from the LDV signal to an adjustable fraction of the total run time.

The 200 kHz input from U83-6 is divided by unit U88 into eight outputs of different frequencies. The comparator U89 selects one of these frequencies according to the status of contacts C, B and A of the multiple switch S4 as summarized in the following table:

C	B	A	Frequency [Hz]
0	0	0	391
0	0	1	195
0	1	0	98
0	1	1	49

1	0	0	24
1	0	1	12
1	1	0	6
1	1	1	3

The selected signal provides the duty cycle frequency at which the time gate for particle sampling is open by the output signal [78] (Enable Particle Stuff). It also drives the 8-bit counter U90. The comparators U91, U93 and the flip-flop U100B keep open the time gate for particle sampling (signal [78]) synchronous with the 200 kHz clock frequency as long as the count in U90 reaches the number selected by the status of the contacts B0, B1, ... B7 of multiple switches S2 and S3. Setting a binary number N = B7 B6 ... B0 (0<=N<256) in S2 and S3 results into opening the time gate for particle sampling for N/256th of the duty cycle period. The reset signal from unit U6-9 of the Control Stuff clears the counter U90 for a new count.

Memory and Buffers

Sheet 6 - Board 2

The input buffers U37, U38, U39 transfer data from the Elapsed Time Counter (ETC) to the memories U43 through U48. The signal [29] (Bubble Time Write Enable) from unit U11-11 of the Control Stuff directs the buffers to send the data and the memory to receive them.

The output buffers U40, U41, U42 are activated sequentially by the signals [1], [2], [3] generated by the counter U17 of the Control Stuff and transfer the data from the memories to the output bus under the control of the signal from the Bubble Address Counter (BAC) U12. When inactive they remain in a high impedance state in order not to affect the output bus.

Memory and Buffers

Sheet 7 - Board 2

The input buffers U49, U50, U51, U61B, U62 transfer data from the Particle Duration Counter (PDC), the Elapsed Time Counter (ETC) and the Zero Crossing Counter (ZCC) to the memories U55 through U60, U61B, U62. The signal [30] (Particle Time Write Enable) from the Control Stuff directs the buffers to send the data and the memory to receive them. Only the 12 most significant bits of the ETC are recorded as particle time data, therefore the time resolution of such measurement is reduced by a factor 2^{12} with respect to the resolution of the recorded bubble time data.

The output buffers U52, U53, U54, U63, U102B are activated sequentially by the signals [4], [5], [6], [7], [8] generated by the counter U17 of the Control Stuff and transfer the data from the memories to the output bus under the control of the signal from the Particle Address Counter (PAC) U16. When inactive they remain in a high impedance state in order not to affect the output bus.

More Memory and Buffers

Sheet 13 - Board 2

The input buffers U101, U102A transfer pressure data from the A/D Converter to the memories U104, U105, U106. The signal [49] (Pressure Data Write Enable) from the Control Stuff directs the buffers to send the data and the memory to receive them.

The output buffers U103, U61A are activated sequentially by the signals [56], [8] generated by the counter U17 of the Control Stuff and transfer the data from the memories to the output bus under the control of the signal from the Particle Address Counter (PAC) U16. When inactive they remain in a high impedance state in order not to affect the output bus.

RS232C Data Interface

Sheet 10 - Board 2

The RS232C data interface accepts 8-bit parallel data from the memory output bus and converts them into RS232C serial format. It is activated by the unload signal [98] synchronized with the 9.6 kHz control clock signal [99] by the gate U77 and is reset by the start load reset signal [50]. The read clock signal [48] increments the Bubble Address Counter (BAC) or the Particle Address Counter (PAC) after each data has been sent to the RS232C serial port. The auxiliary signals [71] (memory reset at run start) and [53] (data unload not under way) prevent accidental data output when not required.

BLOCK DIAGRAM OF C. S. M. INFORMATION FLOW

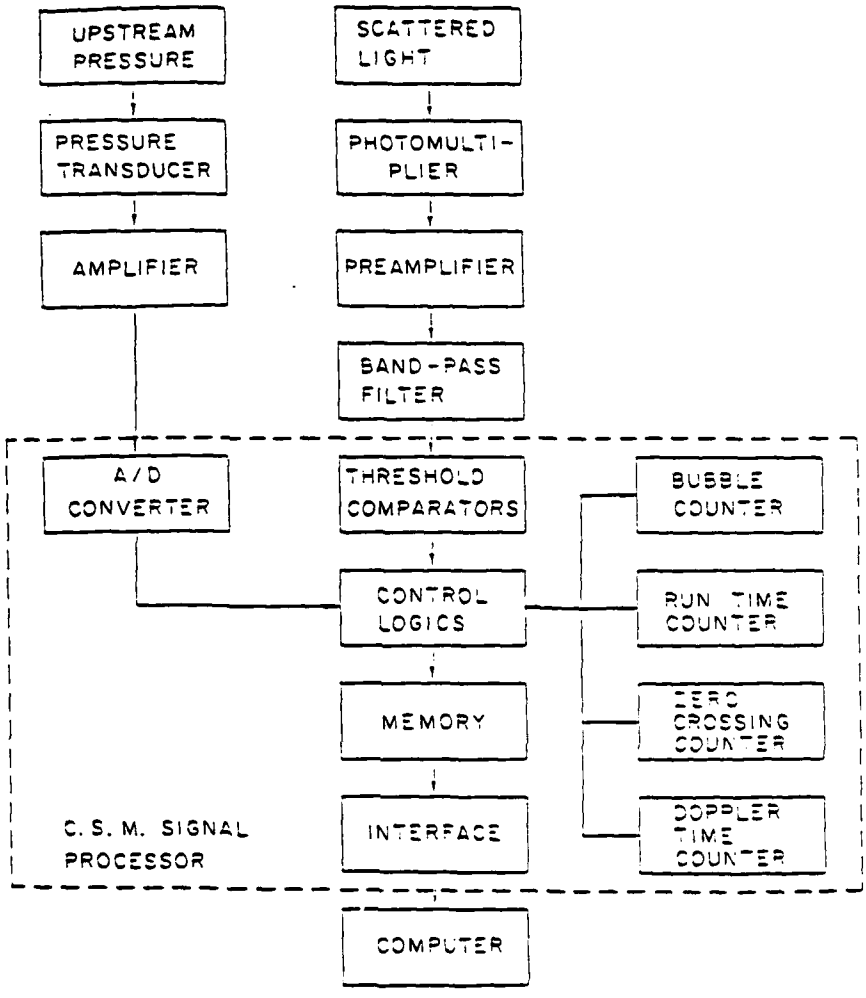

Fig.A-1

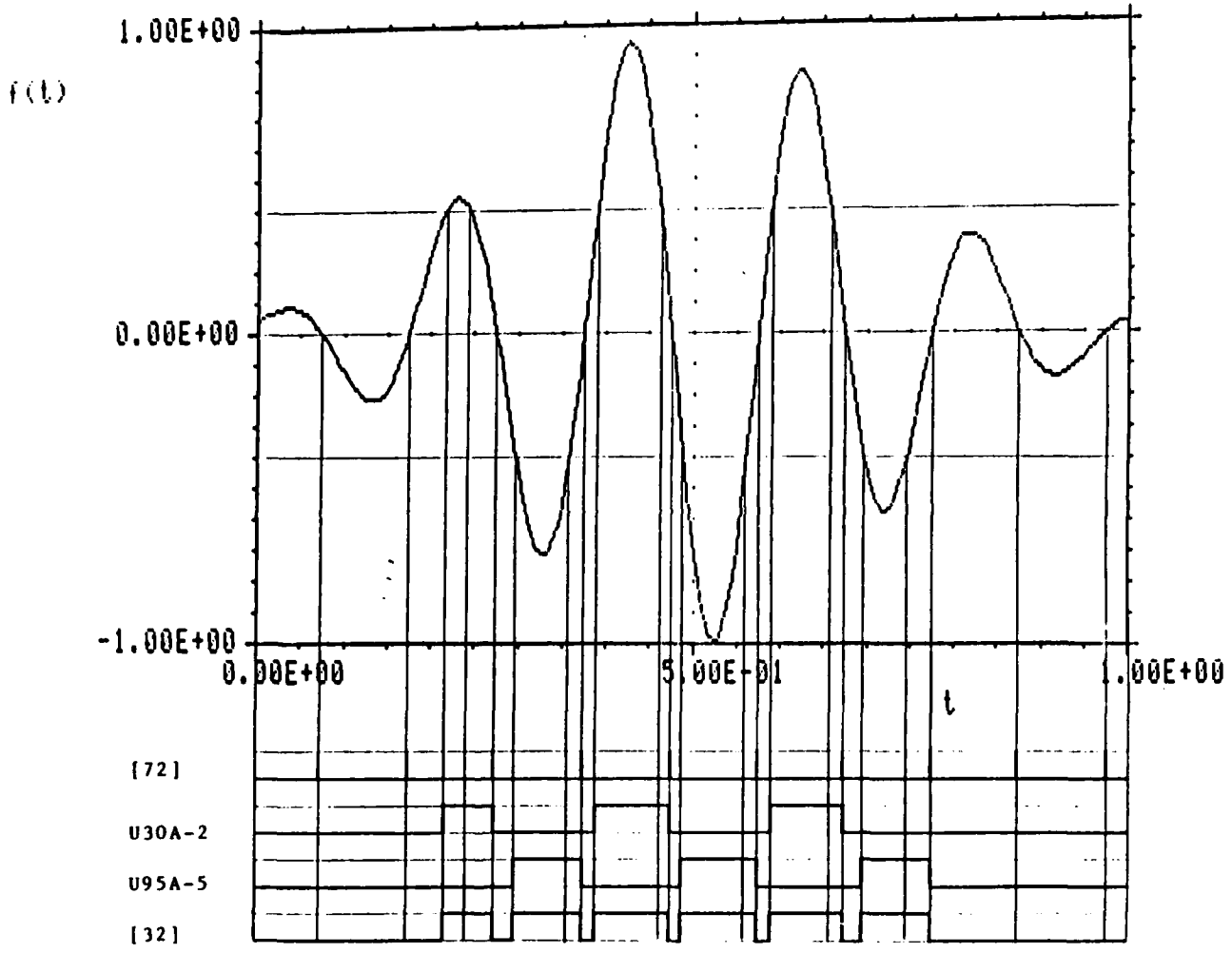
f(t)
1.00E+00
0.00E+00
-1.00E+00
0.00E+00
5.00E-01
1.00E+00
t
[72]
U30A-2
U95A-5
[32]

Fig. A-2

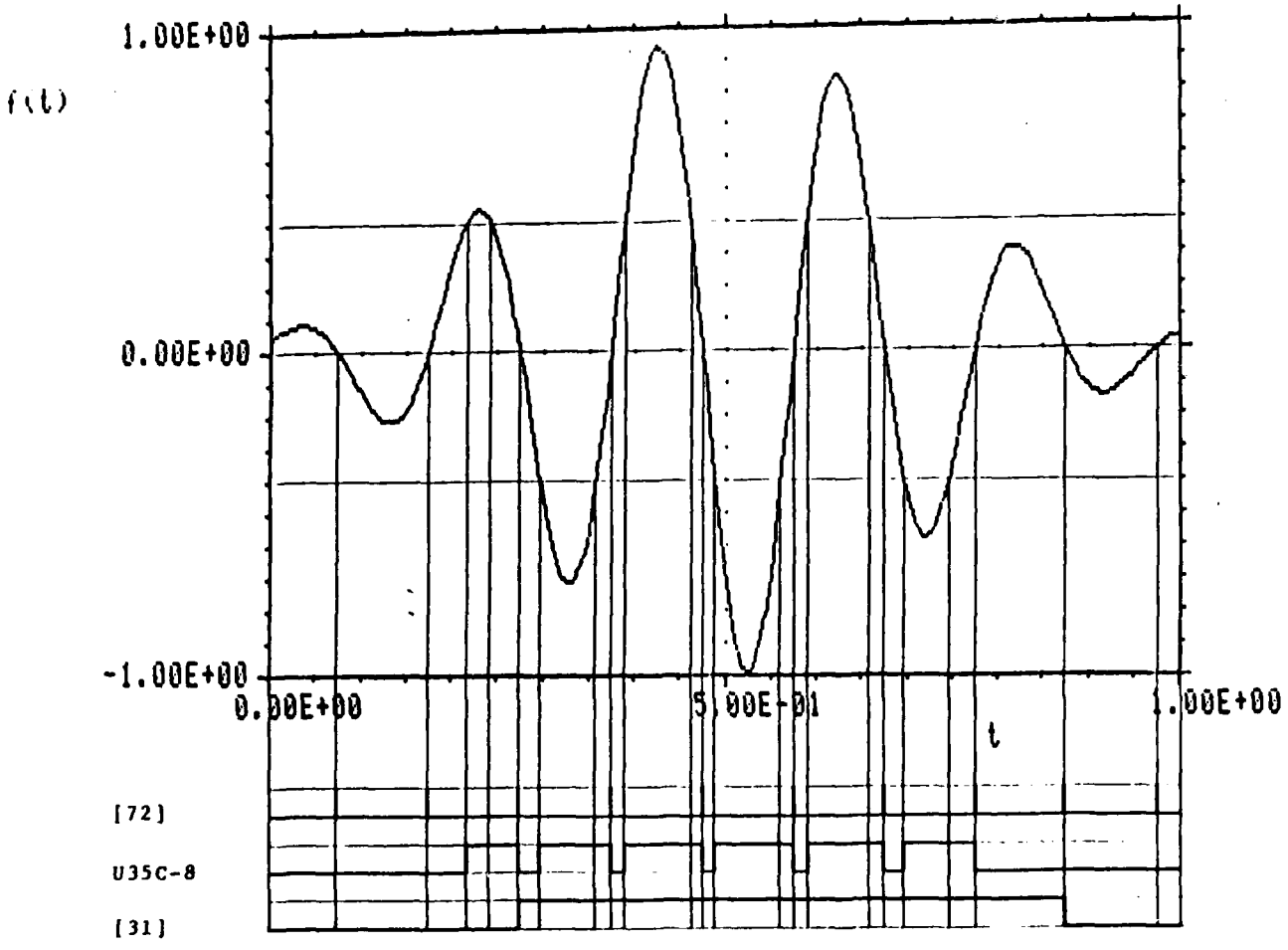

Fig. A-3

Appendix A

Signal Processor Circuit Drawings

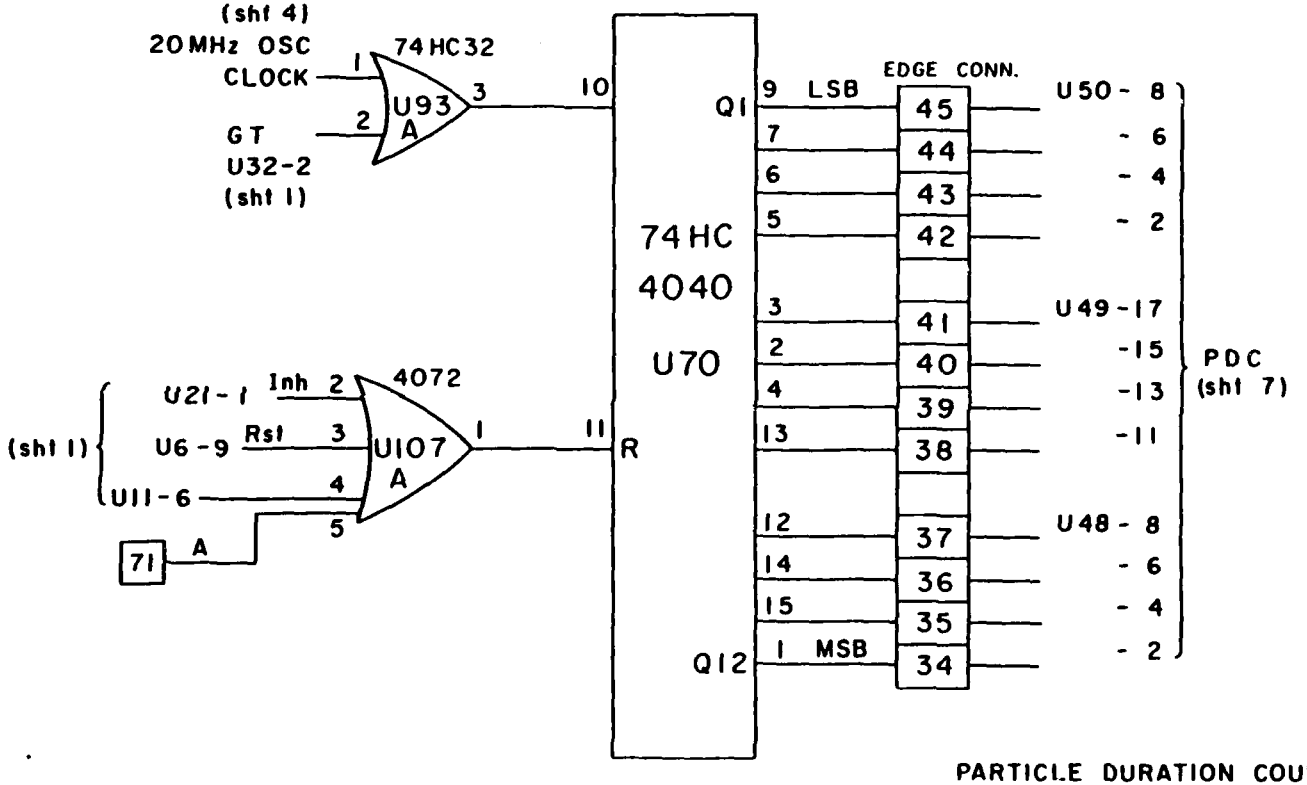

PARTICLE DURATION COUNTER
684
sht 2 of 22

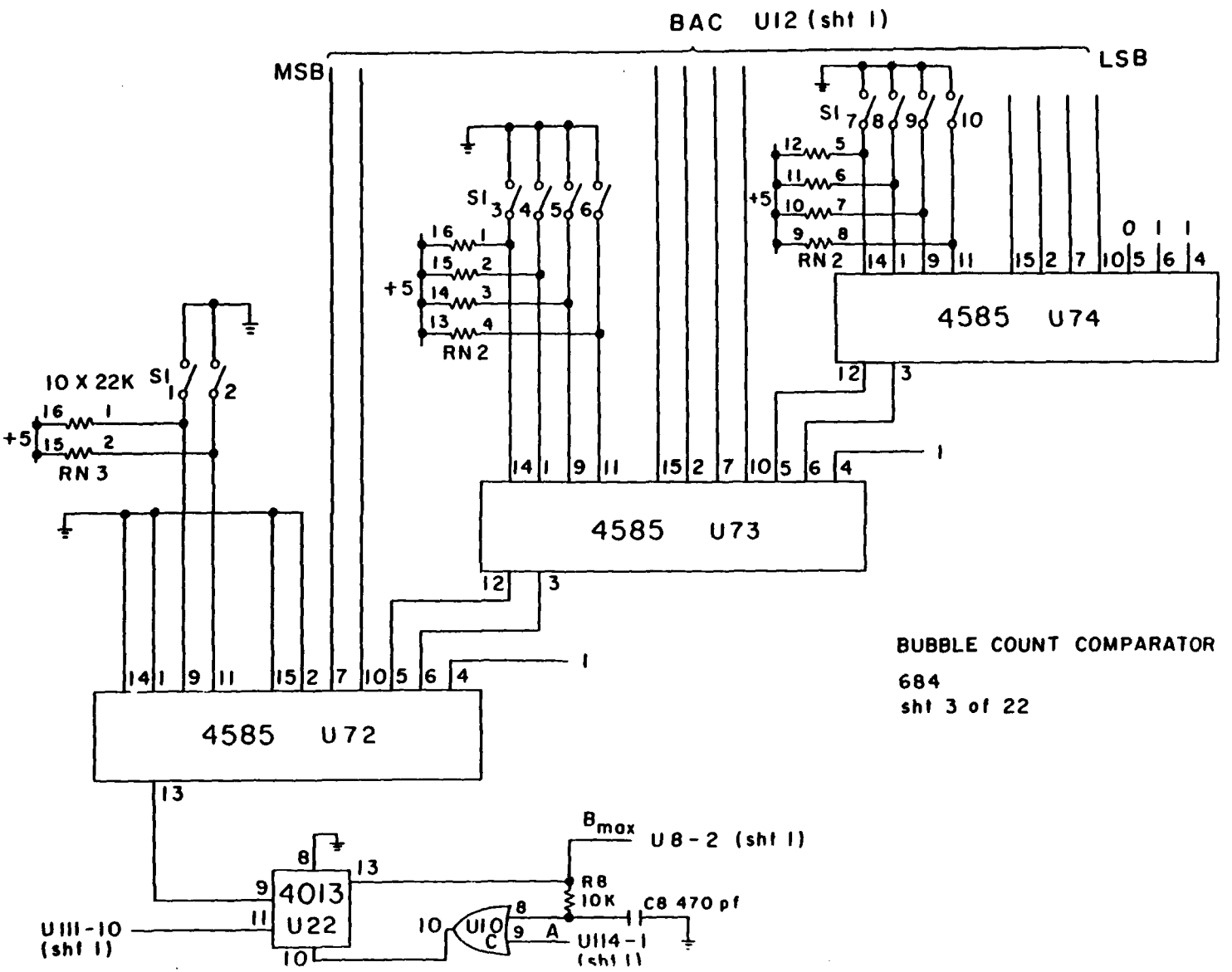
BAC U12 (sht 1)
MSB
LSB
SI
10 X 22K
RN 3
RN 2
4585 U74
4585 U73
4585 U72
0 1 1
BUBBLE COUNT COMPARATOR
684
sht 3 of 22
4013
U22
R8
10K
C8 470 pf
U10
U111-10
(sht 1)
U114-1
(sht 1)
Bmax U8-2 (sht 1)

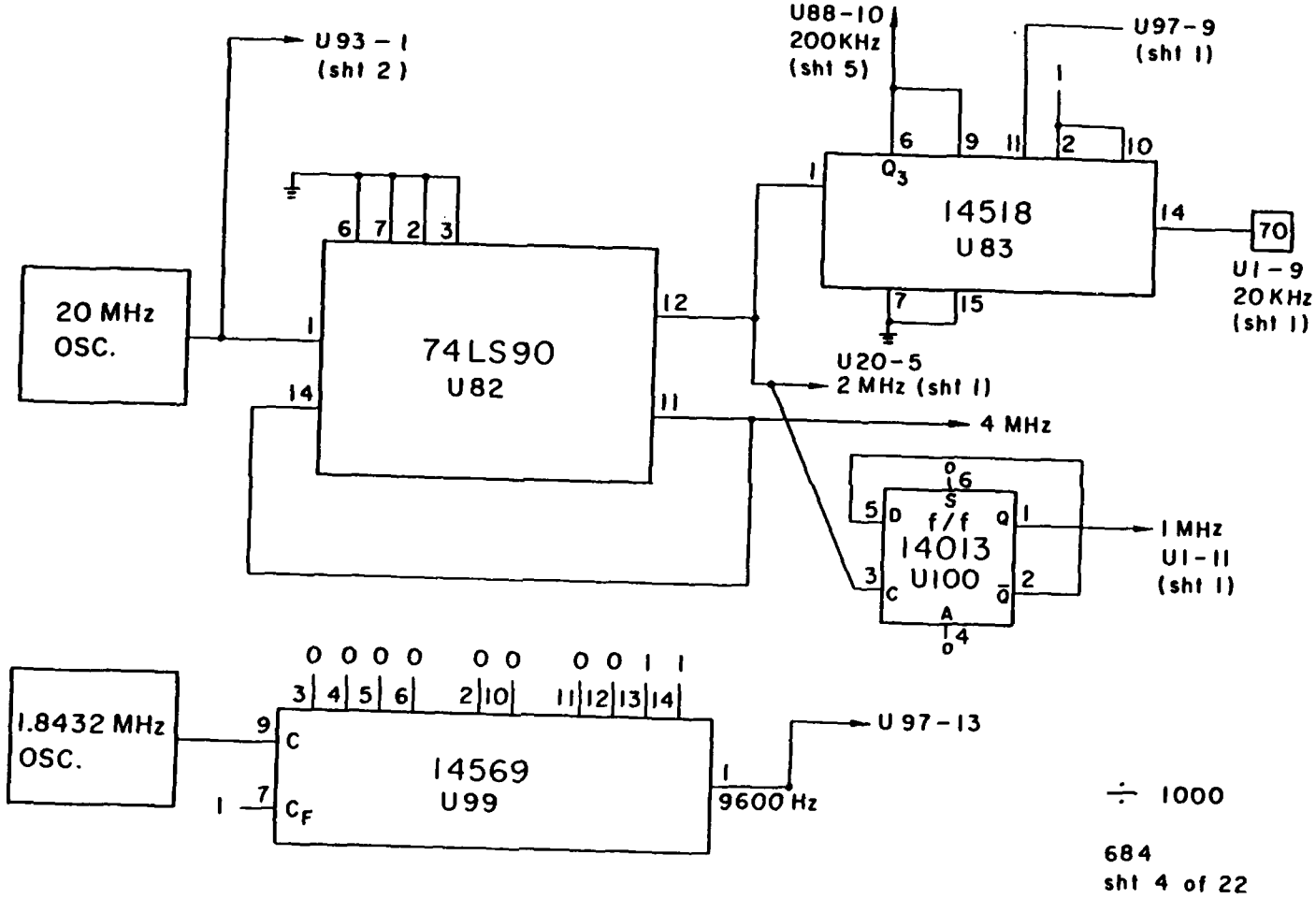
U93 – 1
(sht 2)
U88-10
200KHz
(sht 5)
U97-9
(sht 1)
20 MHz
OSC.
74LS90
U82
14518
U83
70
U1 – 9
20KHz
(sht 1)
U20-5
2 MHz (sht 1)
4 MHz
14013
U100
1 MHz
U1-11
(sht 1)
1.8432 MHz
OSC.
14569
U99
U97-13
9600 Hz
÷ 1000
684
sht 4 of 22

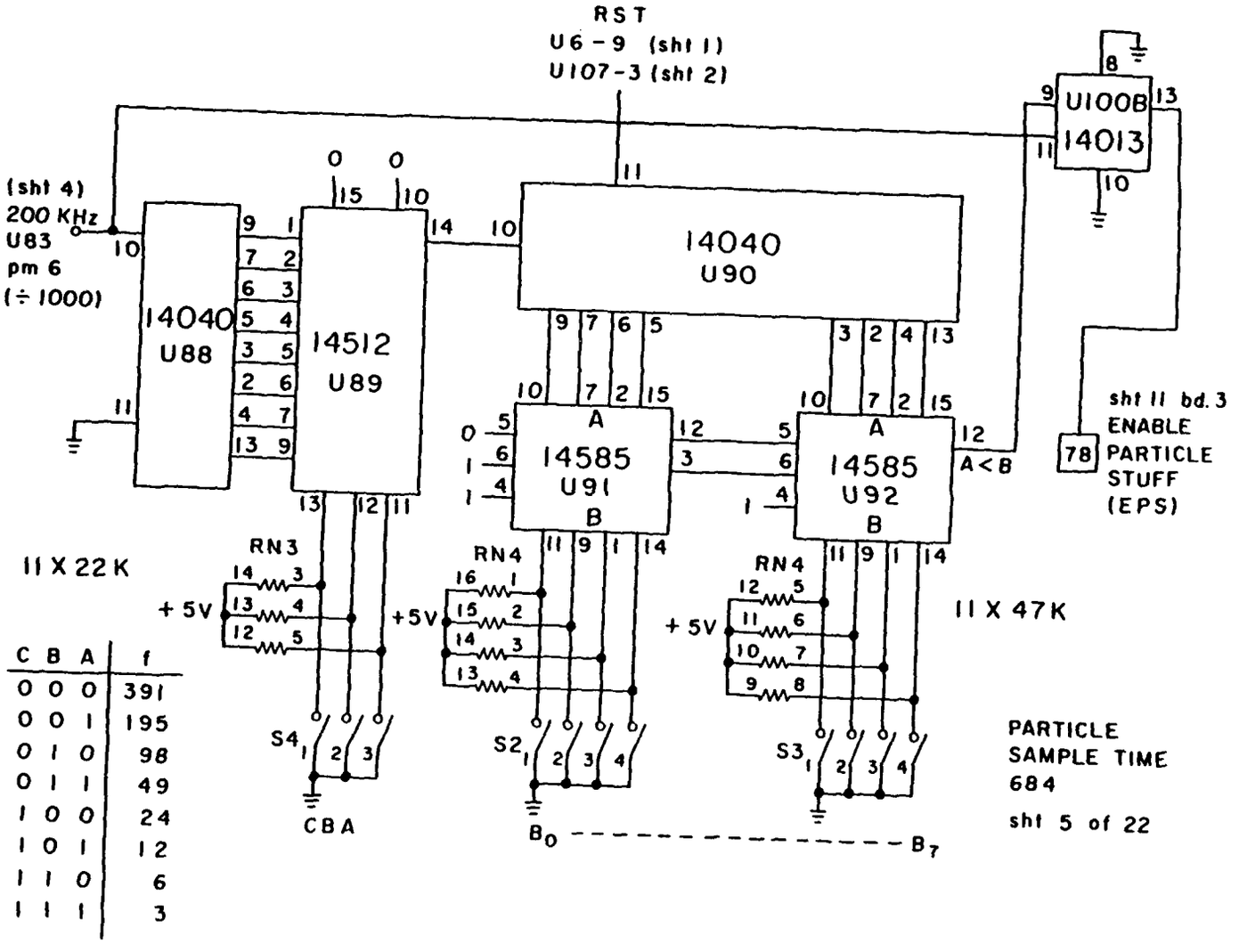

C	B	A	f
0	0	0	391
0	0	1	195
0	1	0	98
0	1	1	49
1	0	0	24
1	0	1	12
1	1	0	6
1	1	1	3

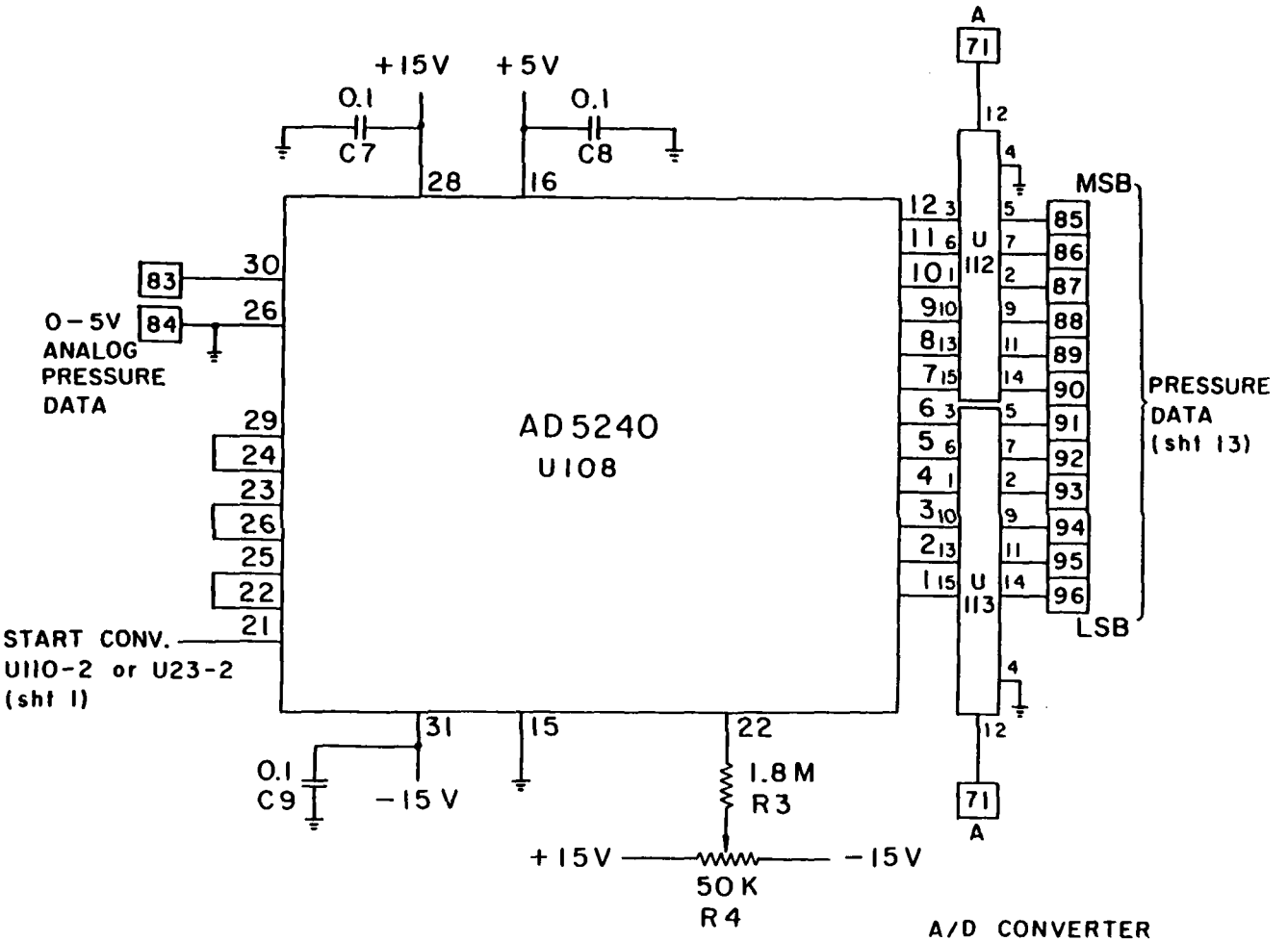
+15V
+5V
0.1
C7
0.1
C8
28
16
30
26
29
24
23
26
25
22
21
31
15
22
AD5240
U108
83
84
0-5V
ANALOG
PRESSURE
DATA
START CONV.
U110-2 or U23-2
(sht 1)
0.1
C9
-15V
1.8M
R3
+15V
-15V
50K
R4
A
71
12
4
U
112
U
113
MSB
LSB
85
86
87
88
89
90
91
92
93
94
95
96
PRESSURE
DATA
(sht 13)
A/D CONVERTER
684
sht 14 of 22

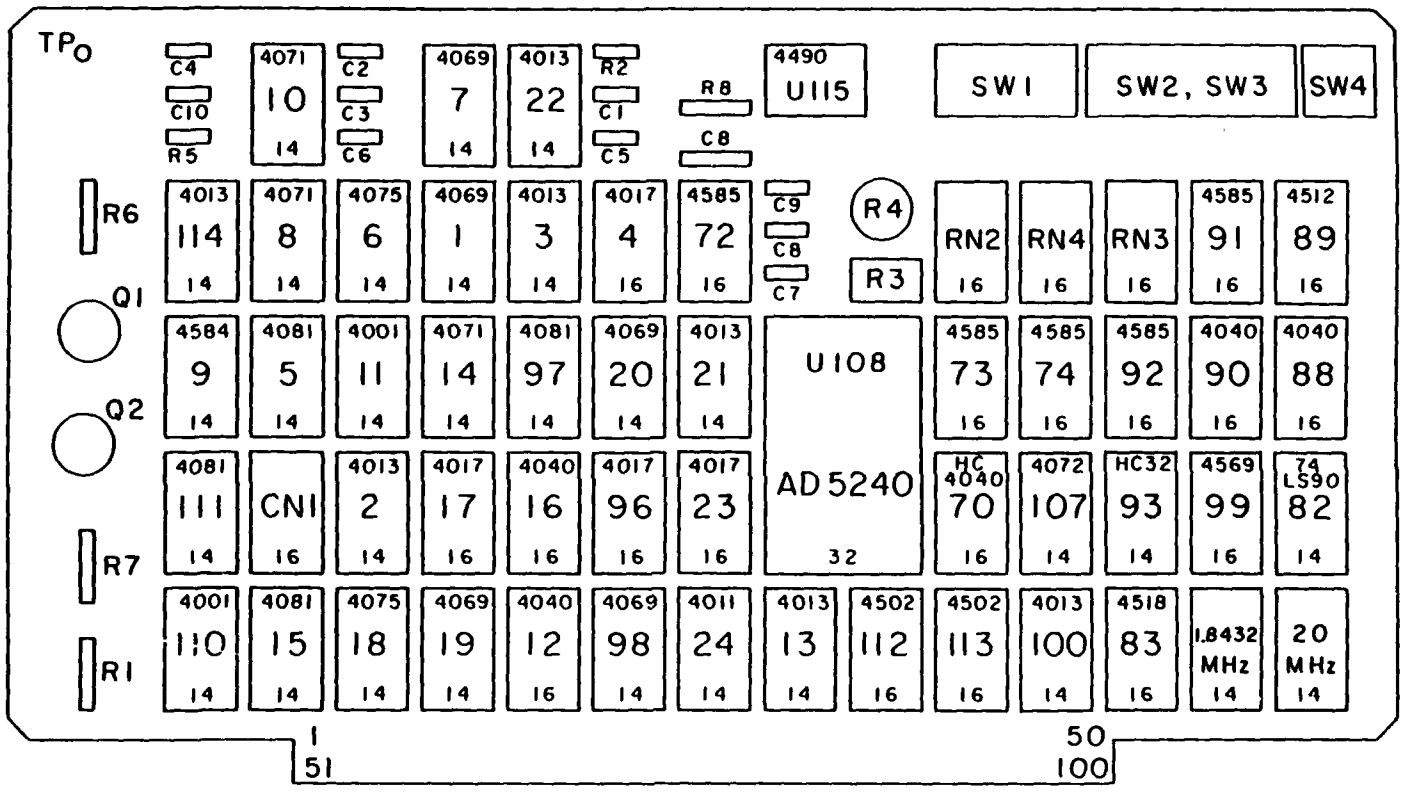

+5V → 58, 59, 60
GND → 51, 75, 100
+15V → 76
−15V → 80

LAYOUT shl 20

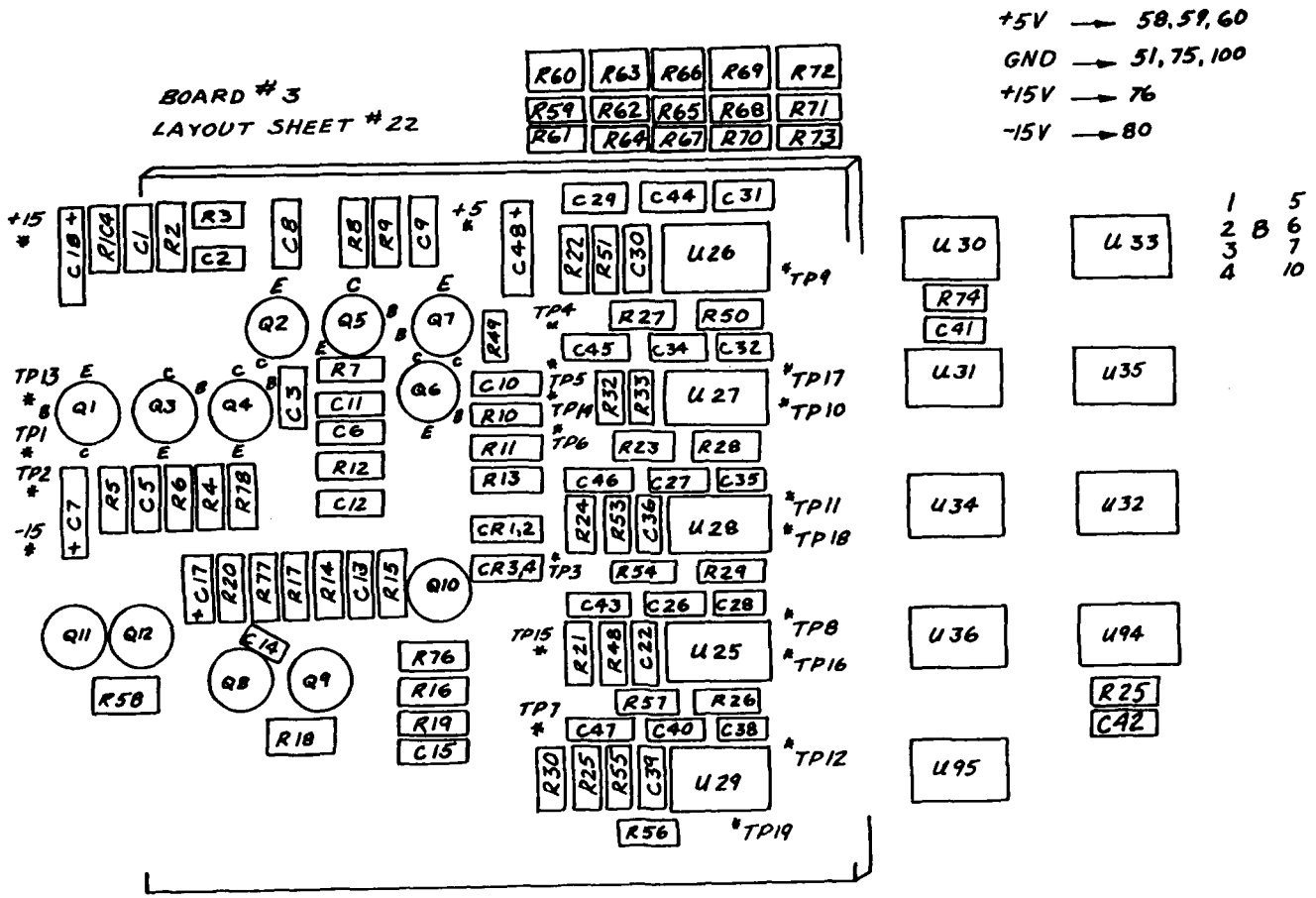
BOARD #3
LAYOUT SHEET #22
+5V → 58, 59, 60
GND → 51, 75, 100
+15V → 76
-15V → 80
R60 R63 R66 R69 R72
R59 R62 R65 R68 R71
R61 R64 R67 R70 R73
C29 C44 C31
U26
U30
U33
U27
U31
U35
U28
U34
U32
U25
U36
U94
U29
U95
Q1 Q2 Q3 Q4 Q5 Q6 Q7 Q8 Q9 Q10 Q11 Q12
TP1 TP2 TP3 TP4 TP5 TP6 TP7 TP8 TP9 TP10 TP11 TP12 TP13 TP15 TP16 TP17 TP18 TP19
+15 -15 +5
1 5
2 B 6
3 7
4 10
BOARD #3

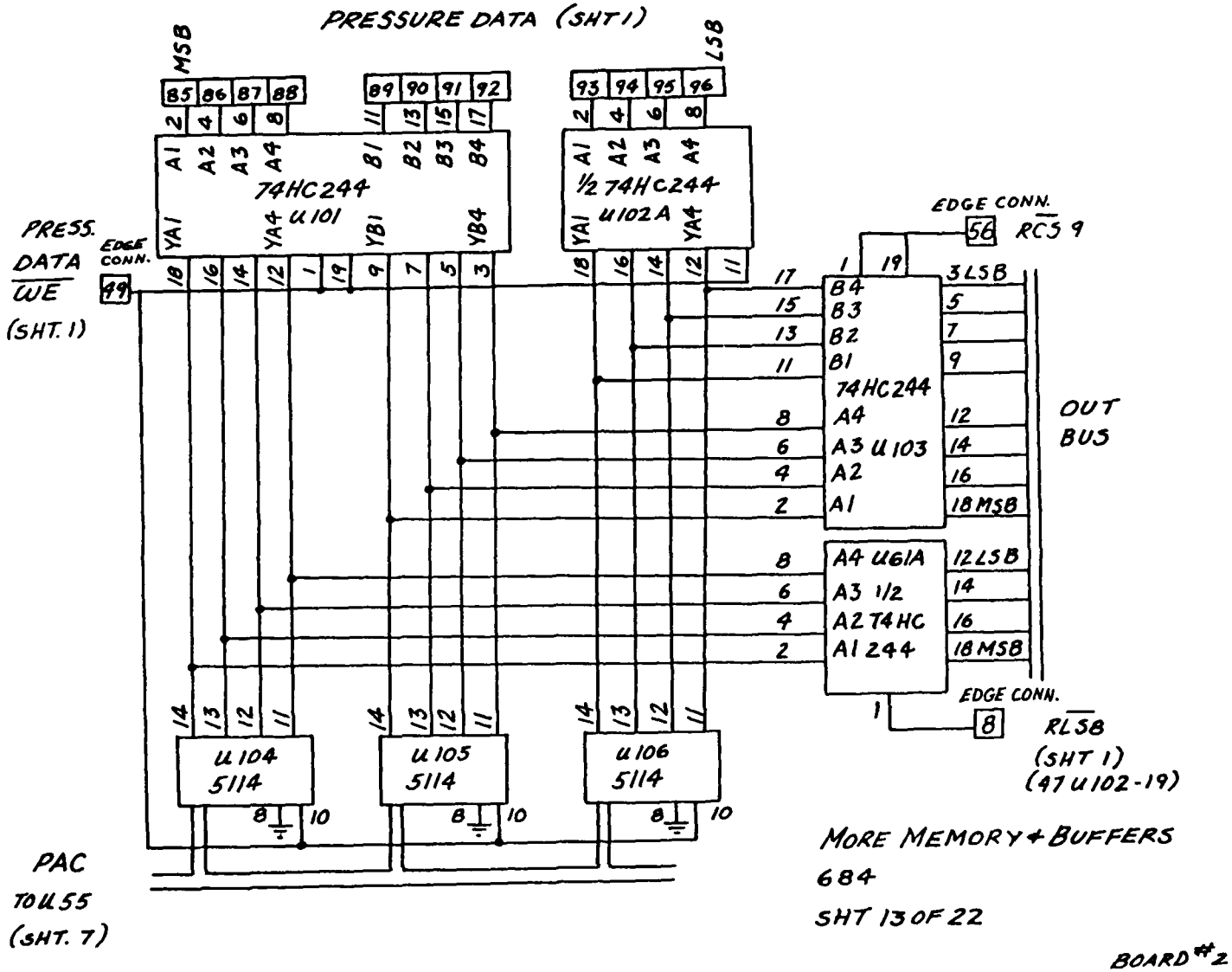
PRESSURE DATA (SHT 1)
MSB
LSB
85 86 87 88
89 90 91 92
93 94 95 96
2 4 6 8
11 13 15 17
A1 A2 A3 A4
B1 B2 B3 B4
74HC244
YA1 YA4 U101
YB1 YB4
½ 74HC244
U102A
PRESS. DATA WE
(SHT. 1)
EDGE CONN.
99
18 16 14 12 1 19 9 7 5 3
EDGE CONN.
56
RC5 9
1 19
17 B4
15 B3
13 B2
11 B1
74HC244
8 A4
6 A3 U103
4 A2
2 A1
3 LSB
5
7
9
12
14
16
18 MSB
OUT BUS
8 A4 U61A
6 A3 1/2
4 A2 74HC
2 A1 244
12 LSB
14
16
18 MSB
EDGE CONN.
1
8
RL5B
(SHT 1)
(47 U102-19)
14 13 12 11
U104 5114
U105 5114
U106 5114
8
10
PAC
TO U55
(SHT. 7)
MORE MEMORY + BUFFERS
684
SHT 13 OF 22
BOARD #2

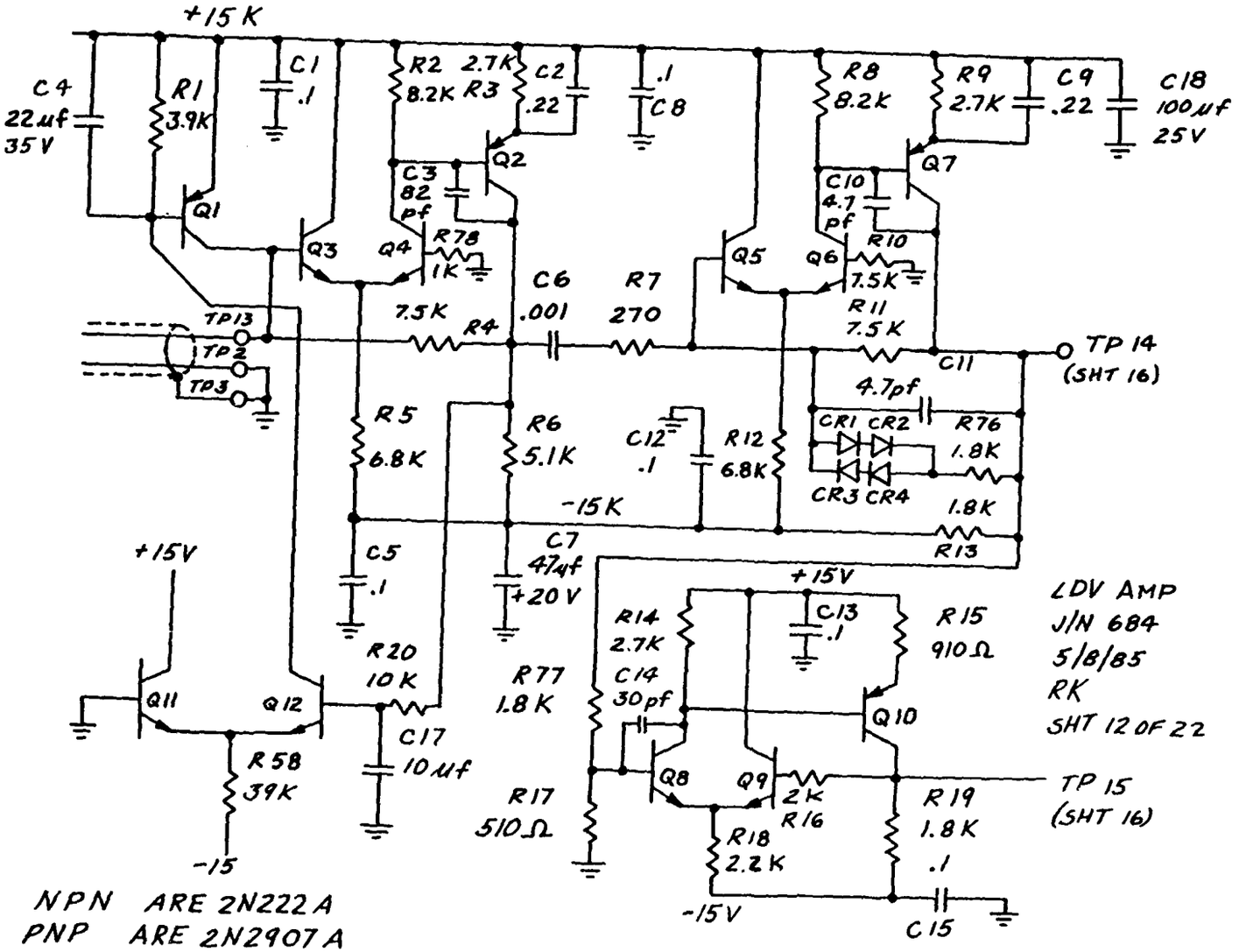
+15 K
C4
22 uf
35 V
R1
3.9K
C1
.1
R2 2.7K
8.2K R3
C2
.22
.1
C8
R8
8.2K
R9
2.7K
C9
.22
C18
100 uf
25 V
Q1
Q2
Q7
C3
82
pf
C10
4.7
pf
Q3
Q4
R78
1K
R10
7.5K
Q5
Q6
C6
.001
R7
270
7.5K
R4
R11
7.5K
TP13
TP2
TP3
TP 14
(SHT 16)
C11
4.7pf
R5
6.8K
R6
5.1K
C12
.1
R12
6.8K
CR1 CR2
R76
1.8K
CR3 CR4
-15K
1.8K
R13
C7
47uf
+20 V
C5
.1
+15V
+15V
R14
2.7K
C13
.1
R15
910 Ω
LDV AMP
J/N 684
5/8/85
RK
SHT 12 OF 22
R20
10K
R77
1.8 K
C14
30pf
Q10
Q11
Q12
C17
10 uf
R58
39K
R17
510 Ω
Q8
Q9
2K
R16
TP 15
(SHT 16)
R18
2.2K
R19
1.8K
.1
-15
-15V
C15
NPN ARE 2N222A
PNP ARE 2N2907A

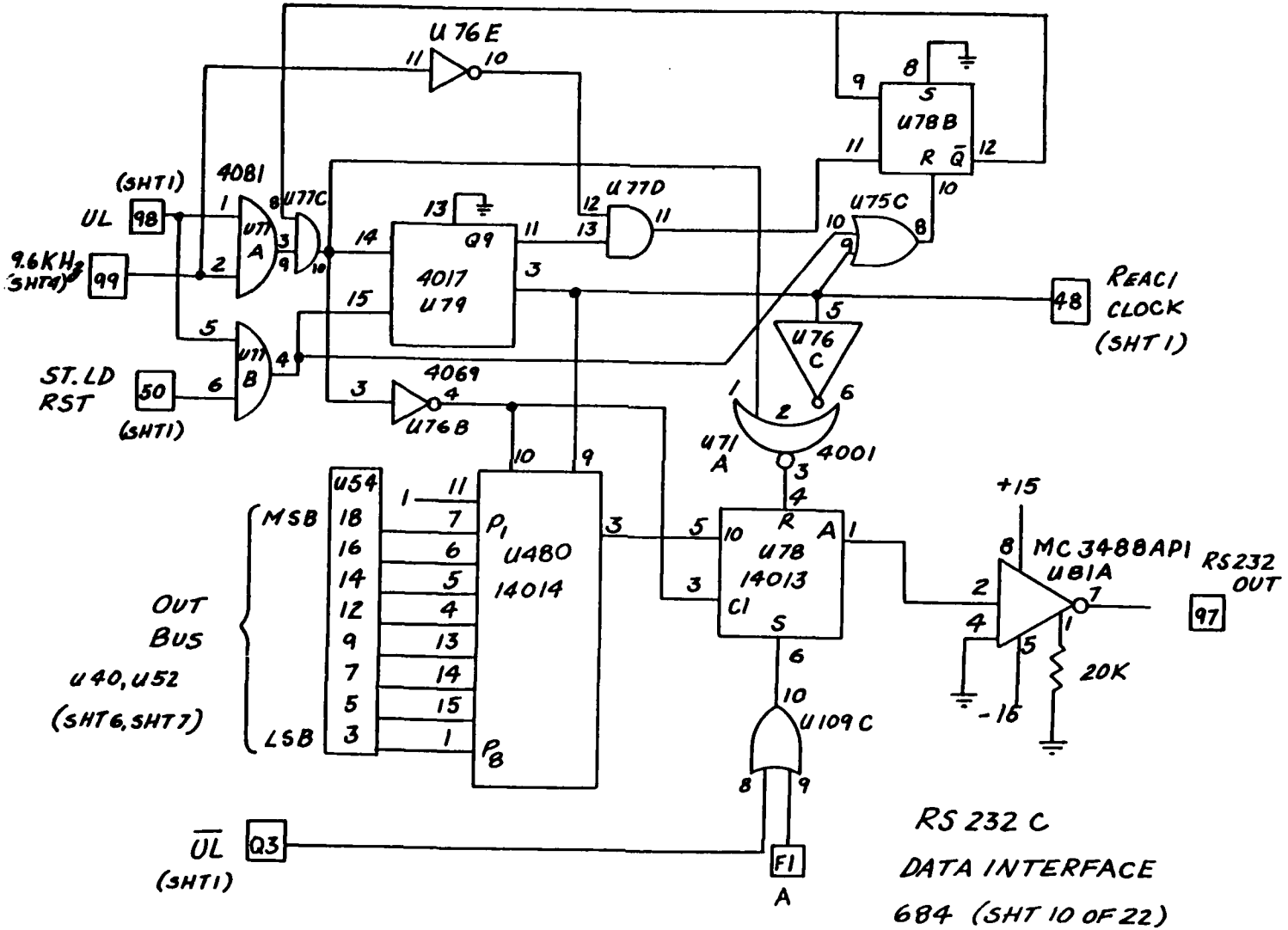
U76E
U78B
U77C
U77D
U75C
U76C
U76B
U71A
U78
U109C
U81A
U480
14014
4017
U79
4081
4069
4001
14013
MC3488API
(SHT1)
UL
98
9.6KHz
(SHT9)
99
ST. LD
RST
50
(SHT1)
4017
U79
Q9
REAC/
CLOCK
48
(SHT 1)
MSB
LSB
OUT
BUS
U40, U52
(SHT6, SHT7)
U54
P1
PB
+15
-16
20K
RS232
OUT
97
UL
(SHT1)
Q3
F1
A
RS 232 C
DATA INTERFACE
684 (SHT 10 OF 22)
BOARD #2

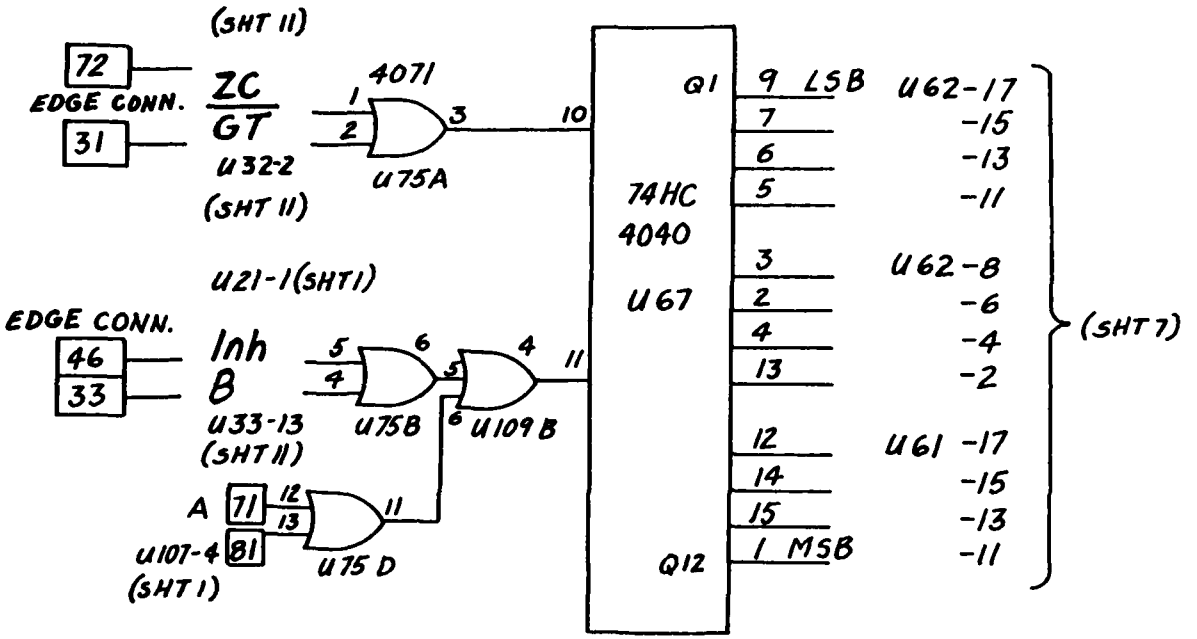

ZERO CROSSING COUNTER

684

SHT 9 OF 22

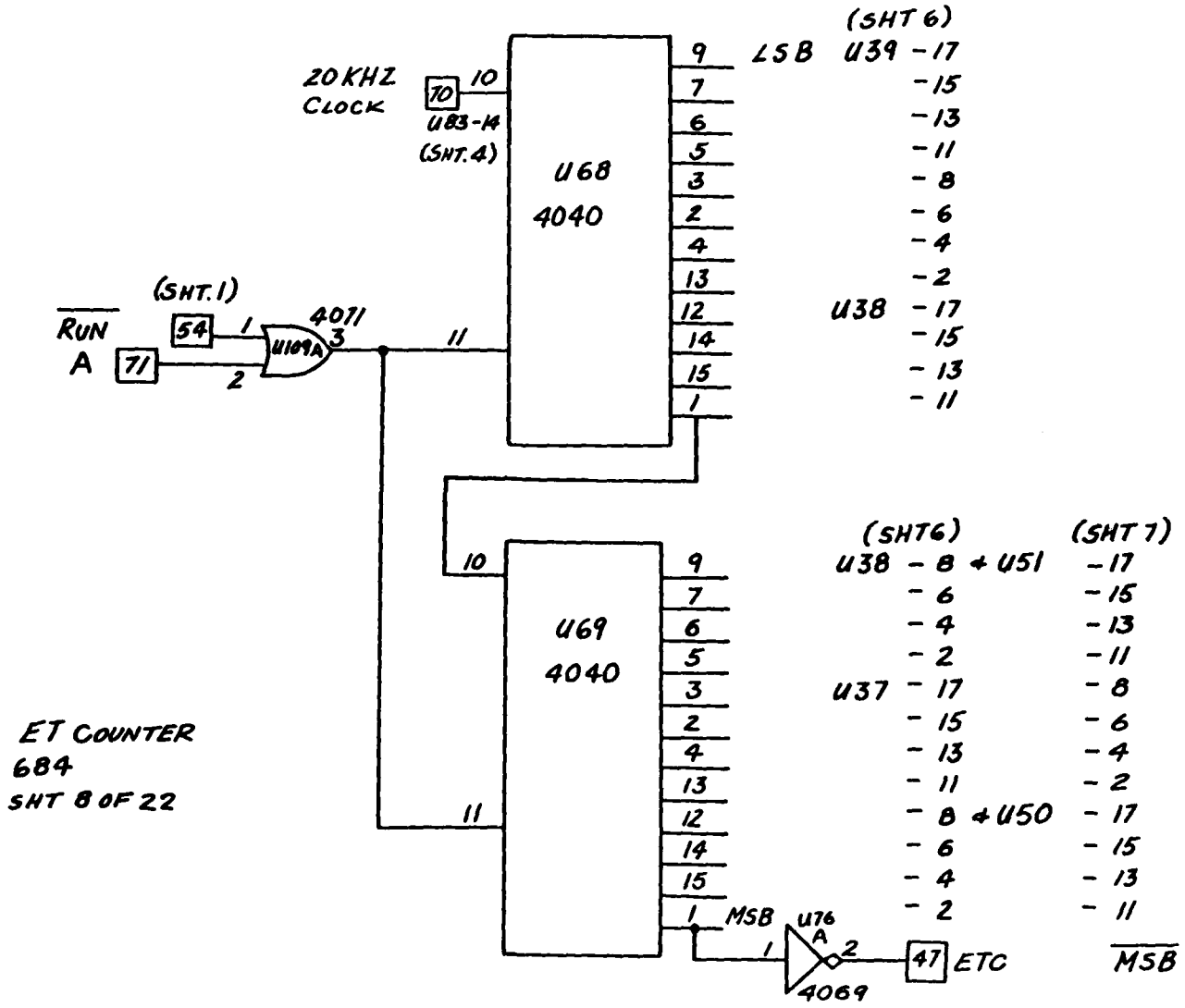
20 KHZ CLOCK
10
70
U83-14 (SHT. 4)
U68 4040
9
7
6
5
3
2
4
13
12
14
15
1
LSB
(SHT 6)
U39 - 17
- 15
- 13
- 11
- 8
- 6
- 4
- 2
U38 - 17
- 15
- 13
- 11
RUN
A
(SHT. 1)
54
71
1
2
U109A
4071
3
11
10
U69 4040
9
7
6
5
3
2
4
13
12
14
15
1
MSB
(SHT6)
U38 - 8 + U51
- 6
- 4
- 2
U37 - 17
- 15
- 13
- 11
- 8 + U50
- 6
- 4
- 2
(SHT 7)
- 17
- 15
- 13
- 11
- 8
- 6
- 4
- 2
- 17
- 15
- 13
- 11
U76 A
1
2
4069
47
ETC
MSB
ET COUNTER
684
SHT 8 OF 22
BOARD #2

BOARD #2
LAYOUT
SHEET 21

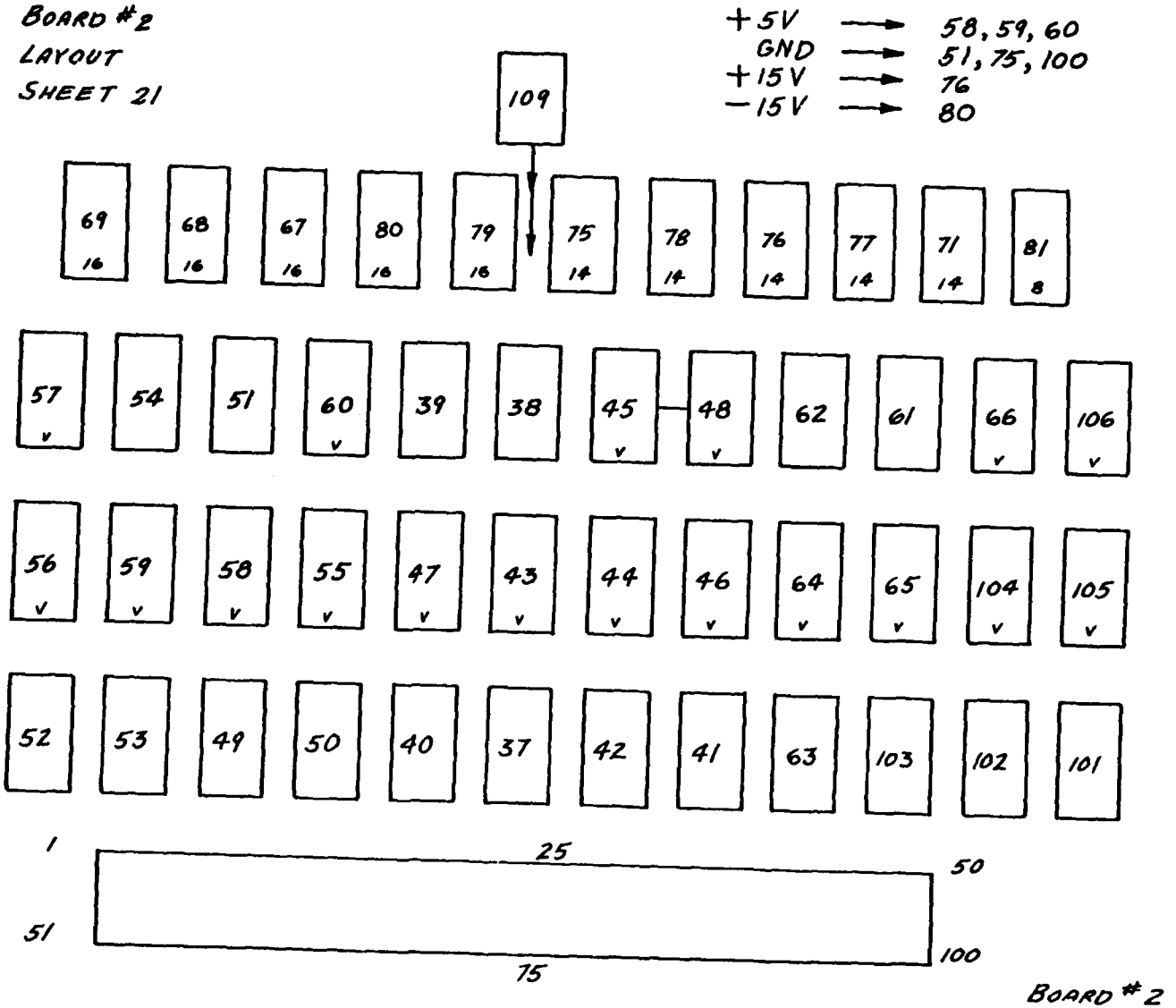

BOARD #2

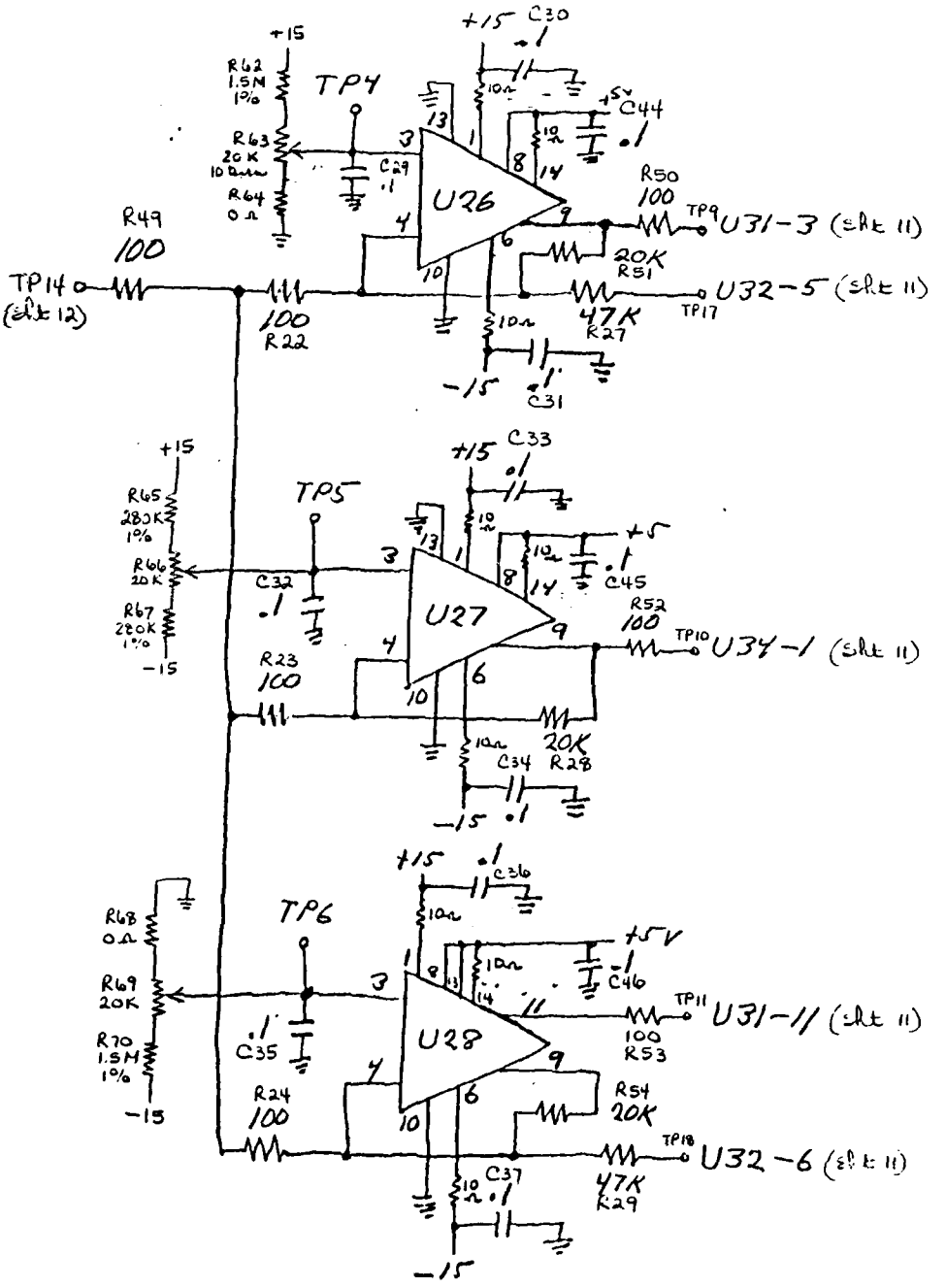

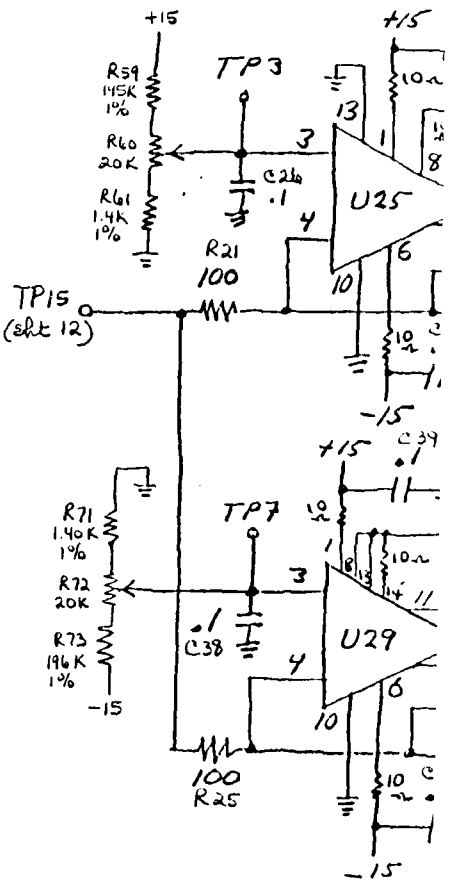

U25 – U29 are LM3

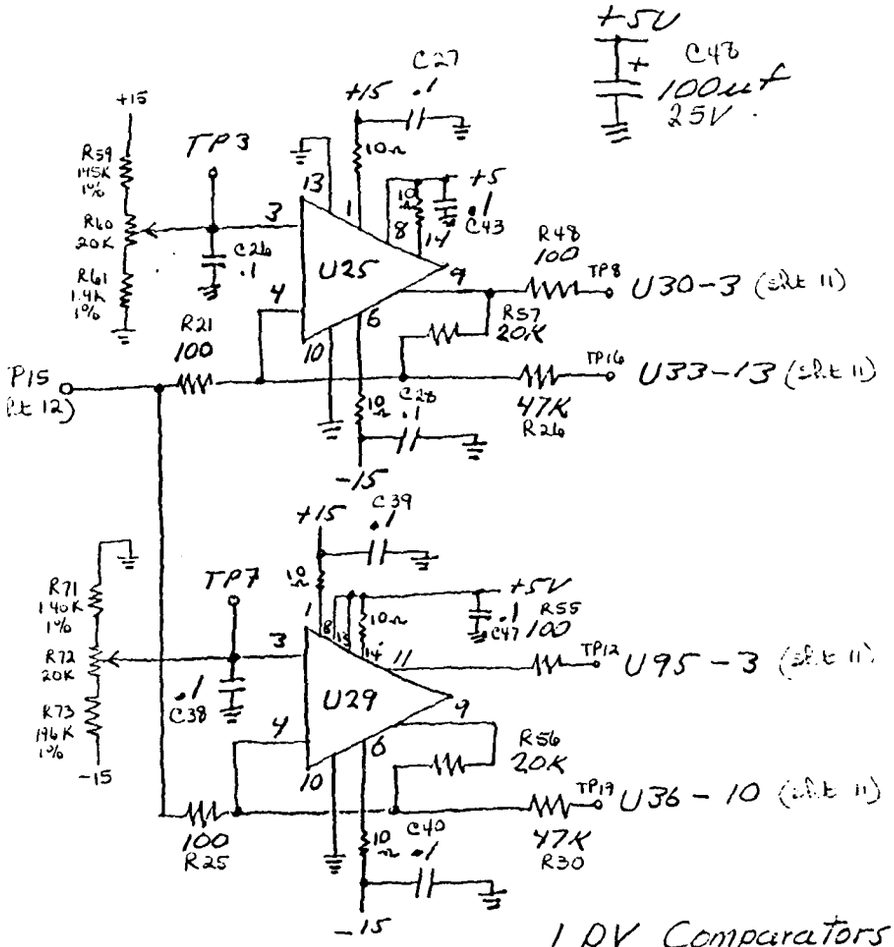

LDV Comparators
J/N 684
5/9/85
RK

U25 – U29 are LM361

Sheet 16 of 22

Revised 10/25 KSB – Add 10Ω decoupling resistors to +5V, +15V & -15V

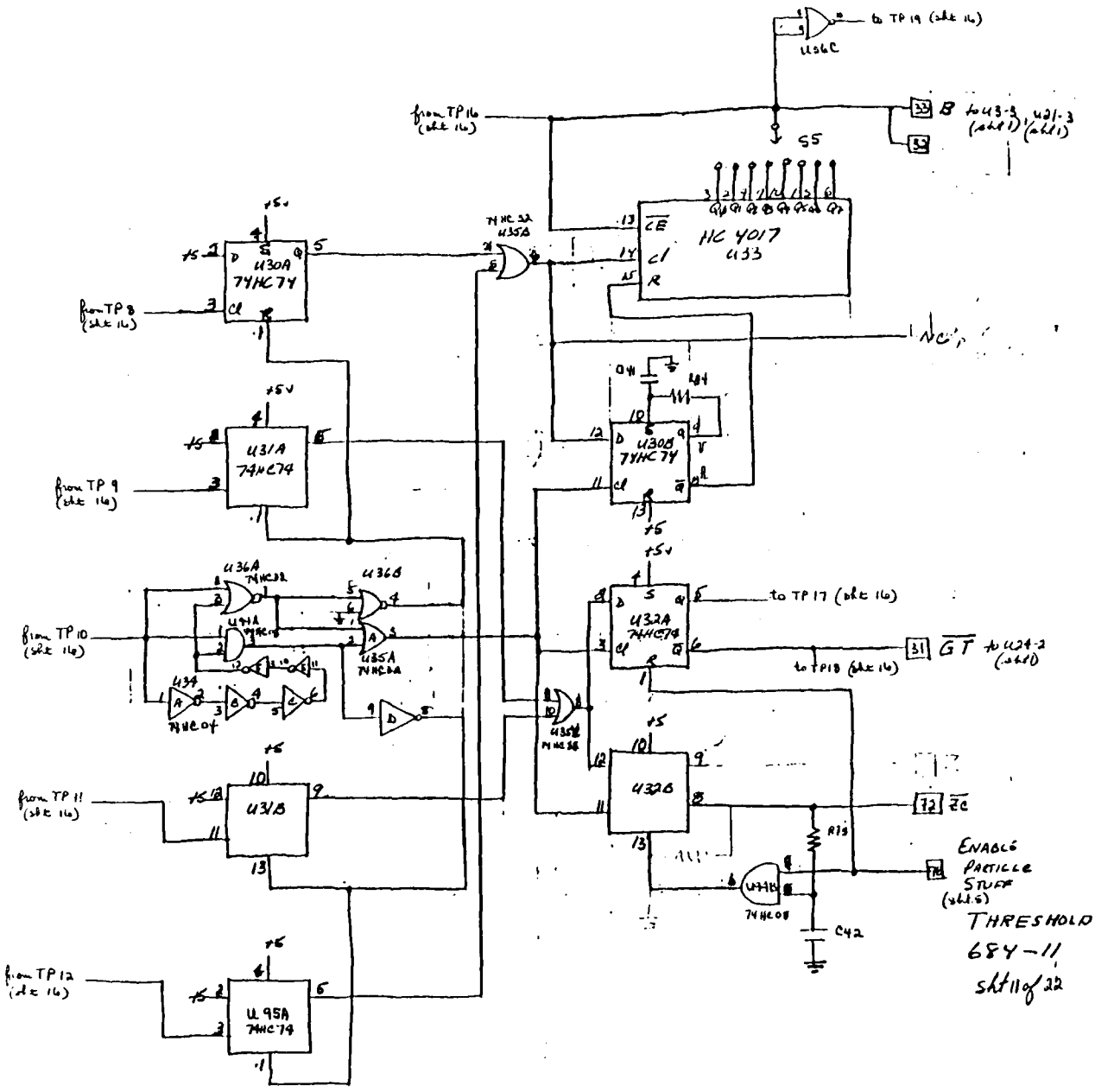
from TP16 (sht 16)
U36C
to TP19 (sht 16)
B to U43-9 (sht 1), U21-3 (sht 1)
55
HC 4017 U33
U30A 74HC74
from TP8 (sht 16)
74HC32 U35A
U30B 74HC74
from TP9 (sht 16)
U31A 74HC74
U36A 74HC32
U36B
U35A 74HC04
from TP10 (sht 16)
U34 74HC04
U32A 74HC74
to TP17 (sht 16)
GT to U24-2 (sht 1)
to TP18 (sht 16)
U35B 74HC32
U32B
from TP11 (sht 16)
U31B
ZC
R13
ENABLE PARTICLE STUFF (sht 16)
U33B 74HC08
C42
from TP12 (sht 16)
U95A 74HC74
THRESHOLD CIRCUITS
684-11
sht 11 of 22
BOARD # 5

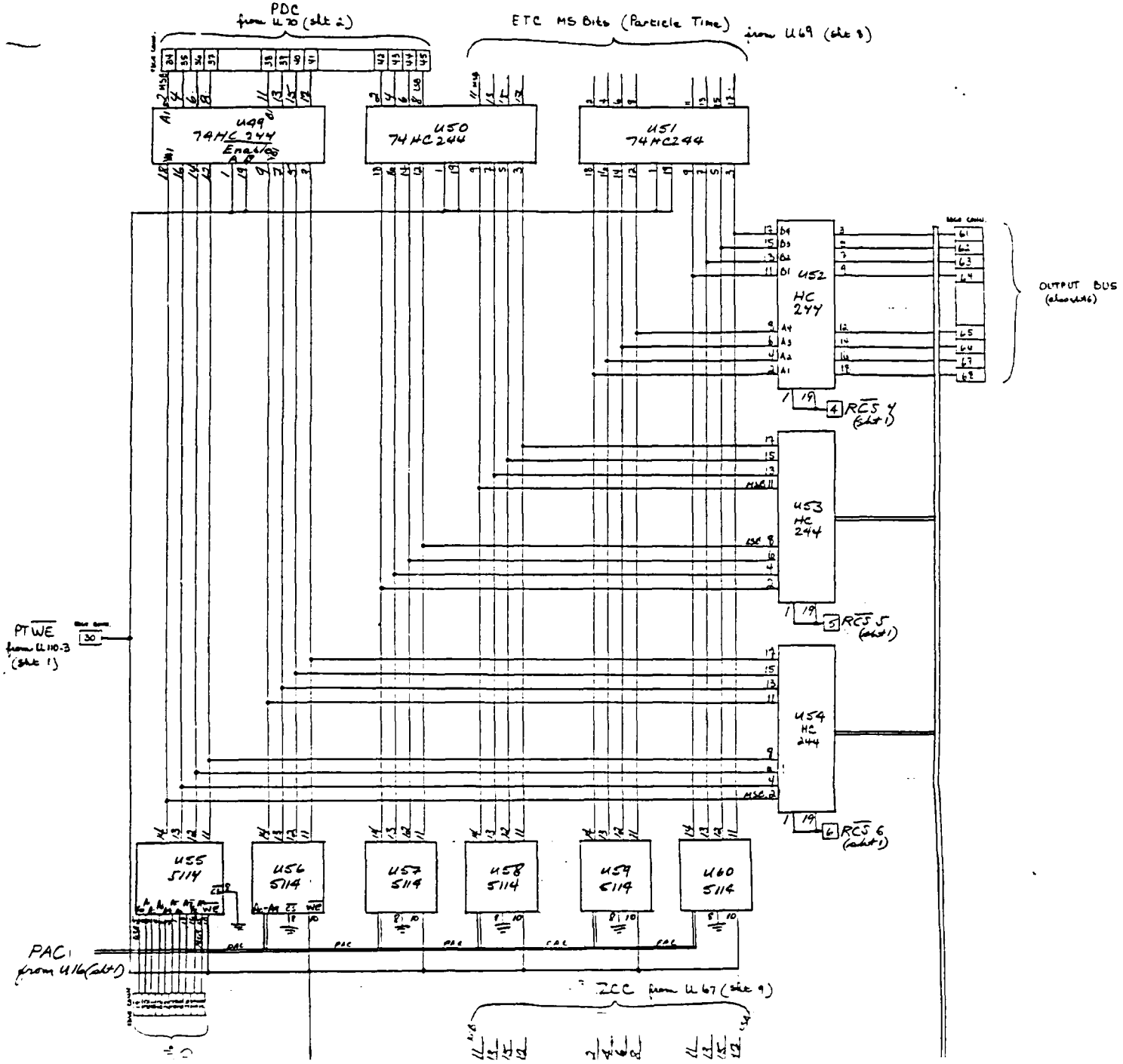
PDC
from U70 (slt 2)
ETC MS Bits (Particle Time)
from U69 (slt 8)
U49
74HC 244
U50
74HC244
U51
74HC244
U52
HC
244
U53
HC
244
U54
HC
244
OUTPUT BUS
(also U46)
RCS 4 (slot 1)
RCS 5 (slot 1)
RCS 6 (slot 1)
PTWE
from U110-3
(slt 1)
U55
5114
U56
5114
U57
5114
U58
5114
U59
5114
U60
5114
PAC
from U16(slot 1)
ZCC from U67 (slt 9)

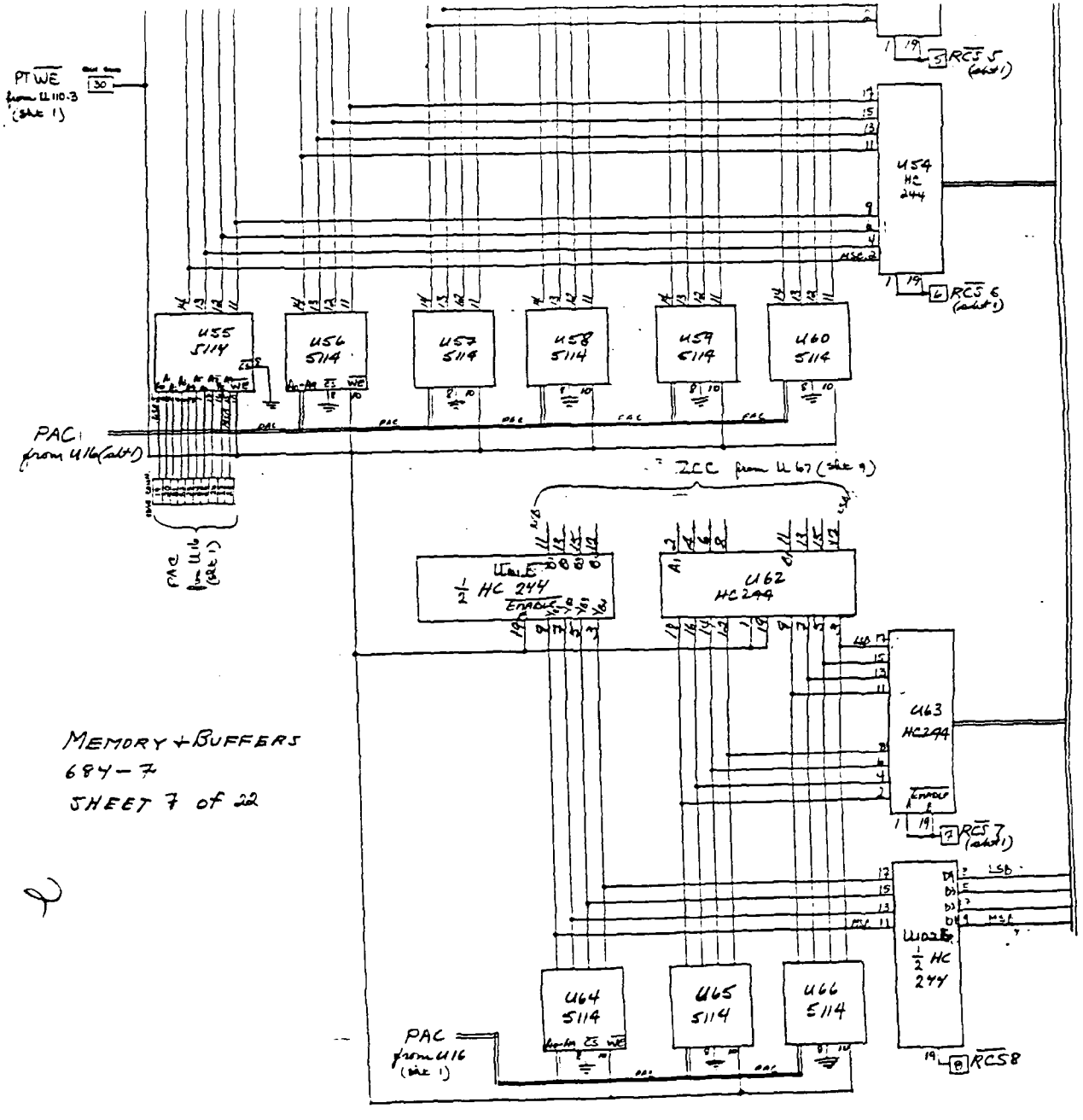

MEMORY + BUFFERS
684-7
SHEET 7 of 22

BOARD #2

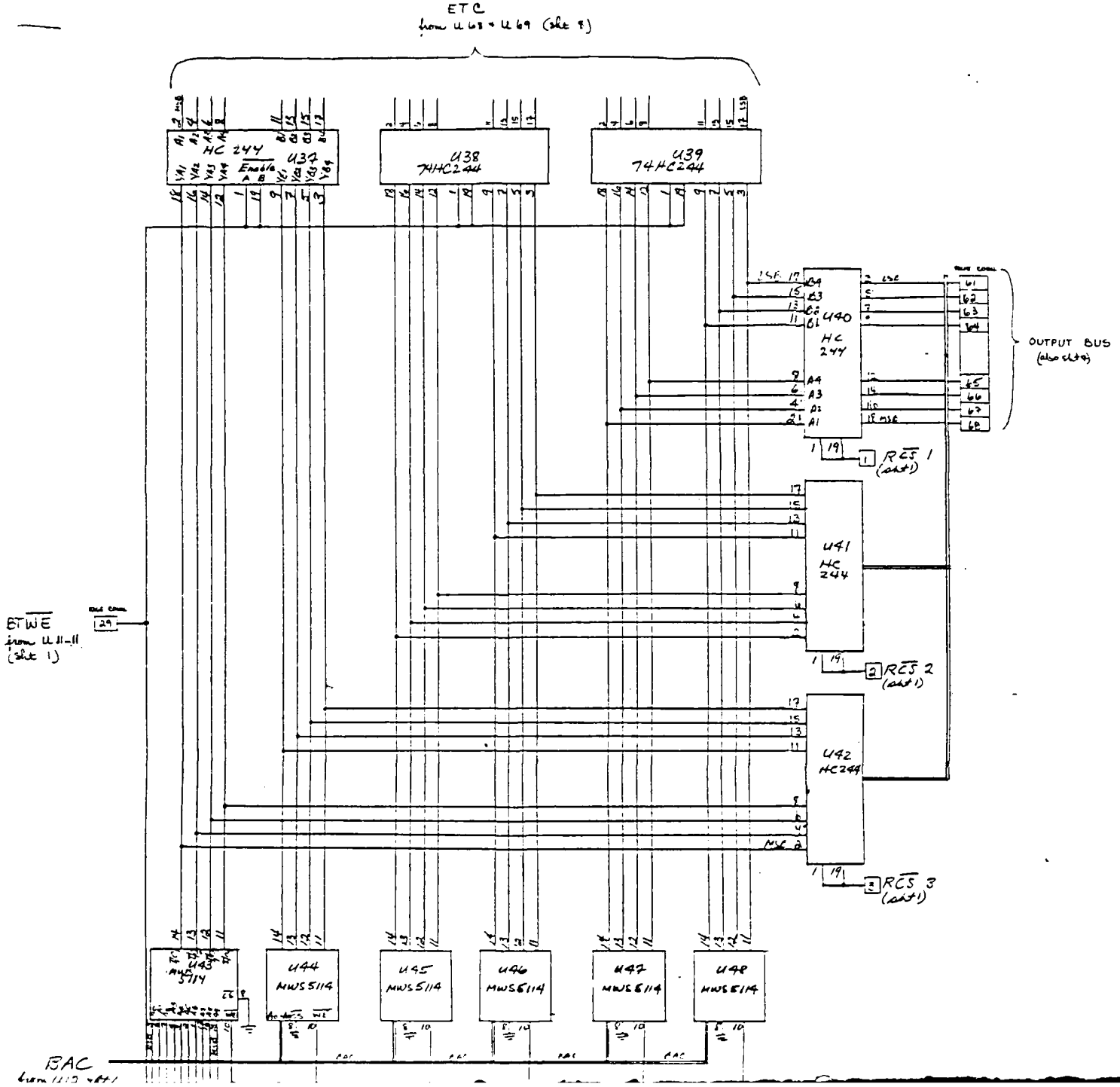
ETC
from U63 + U69 (sht 9)
U37 HC 244
U38 74HC244
U39 74HC244
U40 HC 244
U41 HC 244
U42 HC244
OUTPUT BUS
(also U43)
RCS 1 (cont)
RCS 2 (cont)
RCS 3 (cont)
ETWE
from U11-11 (sht 1)
U43 MWS5114
U44 MWS5114
U45 MWS5114
U46 MWS6114
U47 MWS6114
U48 MWS6114
BAC

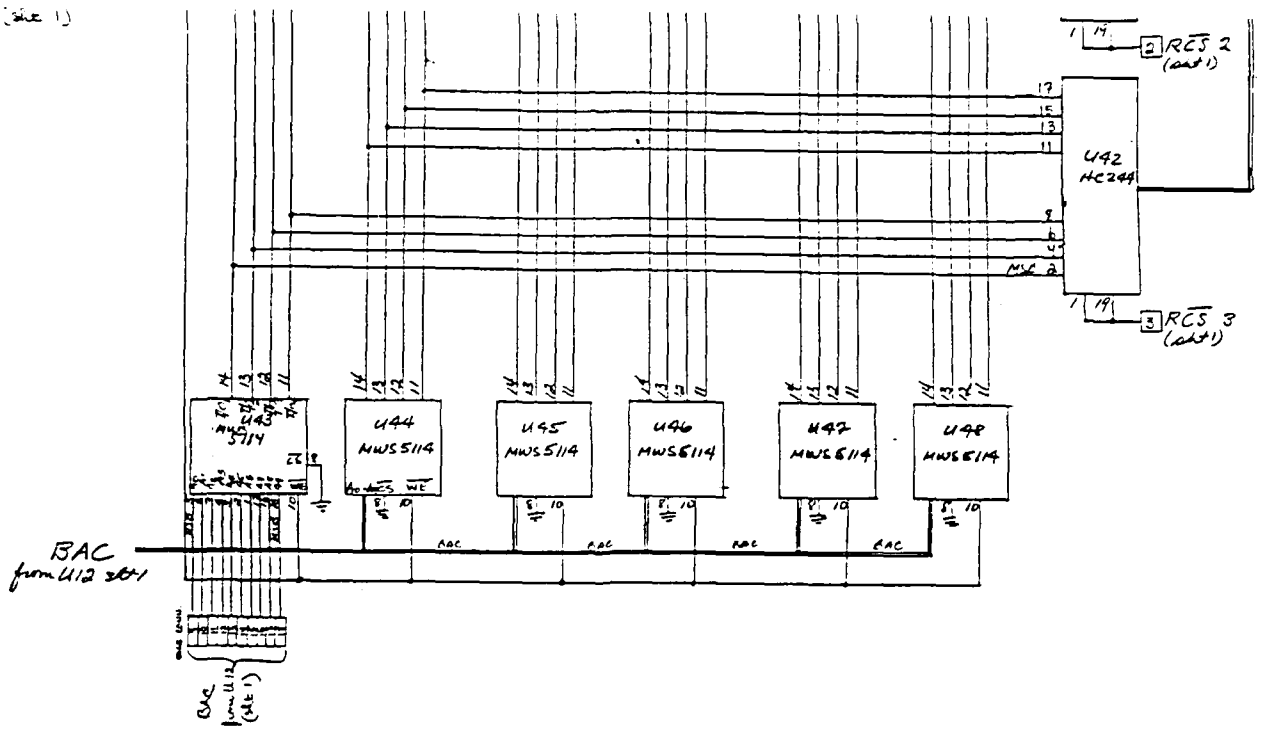

MEMORY + BUFFERS
684-Q
Sheet 6 of 22

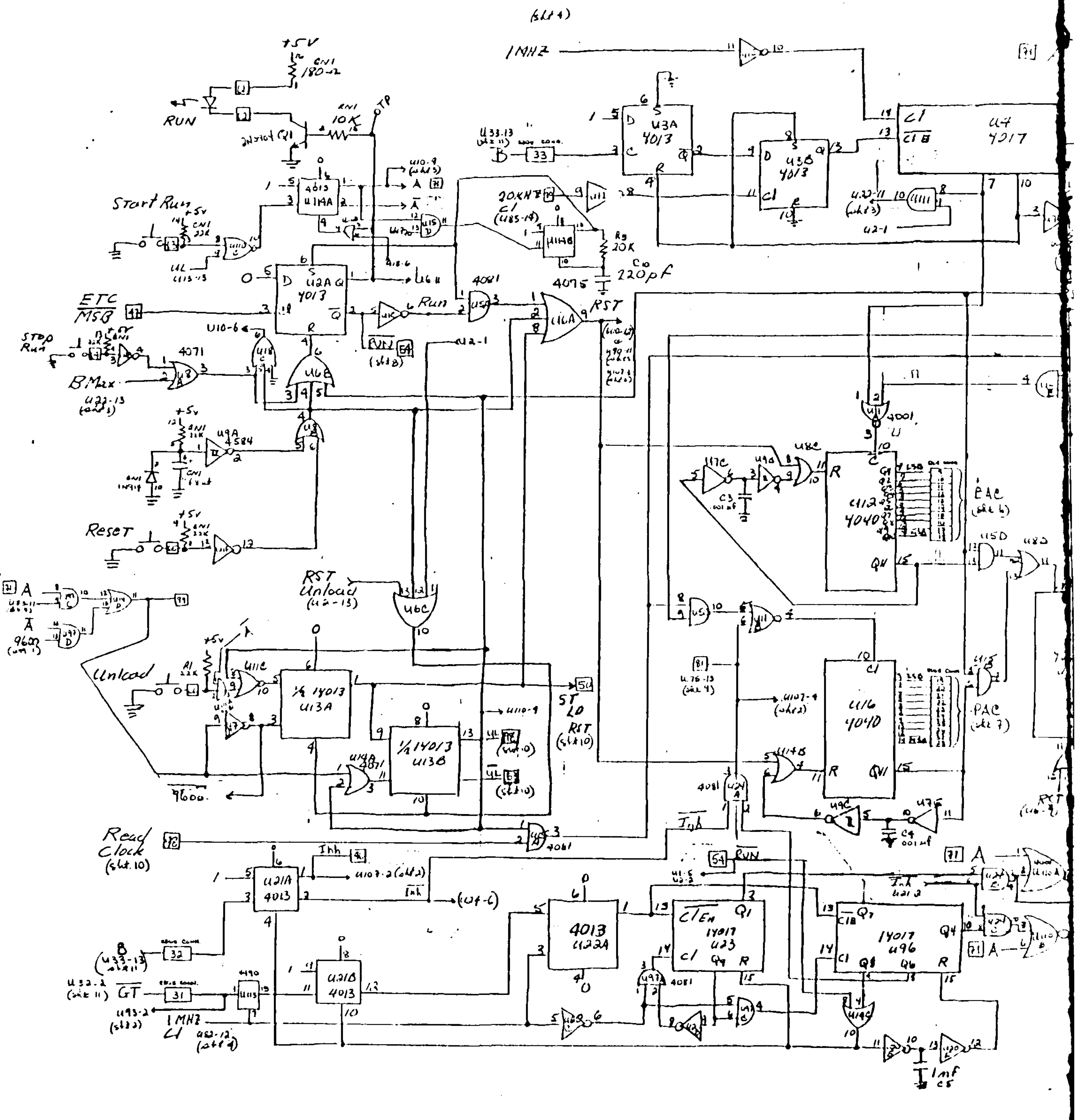

1MHZ
+5V
RUN
Start Run
ETC
MSB
Stop Run
B Max
Reset
4071
4013
4017
4040
4081
4075
220pf
20K
U3A
U4
U12A
U14A
U16
4040
Run
RST
EAC
PAC
Unload
RST Unload
9600
ST LO
Read Clock
U21A
U21B
U22A
U23
U96
4013
14017
GT
1MHZ
Inh
1mf

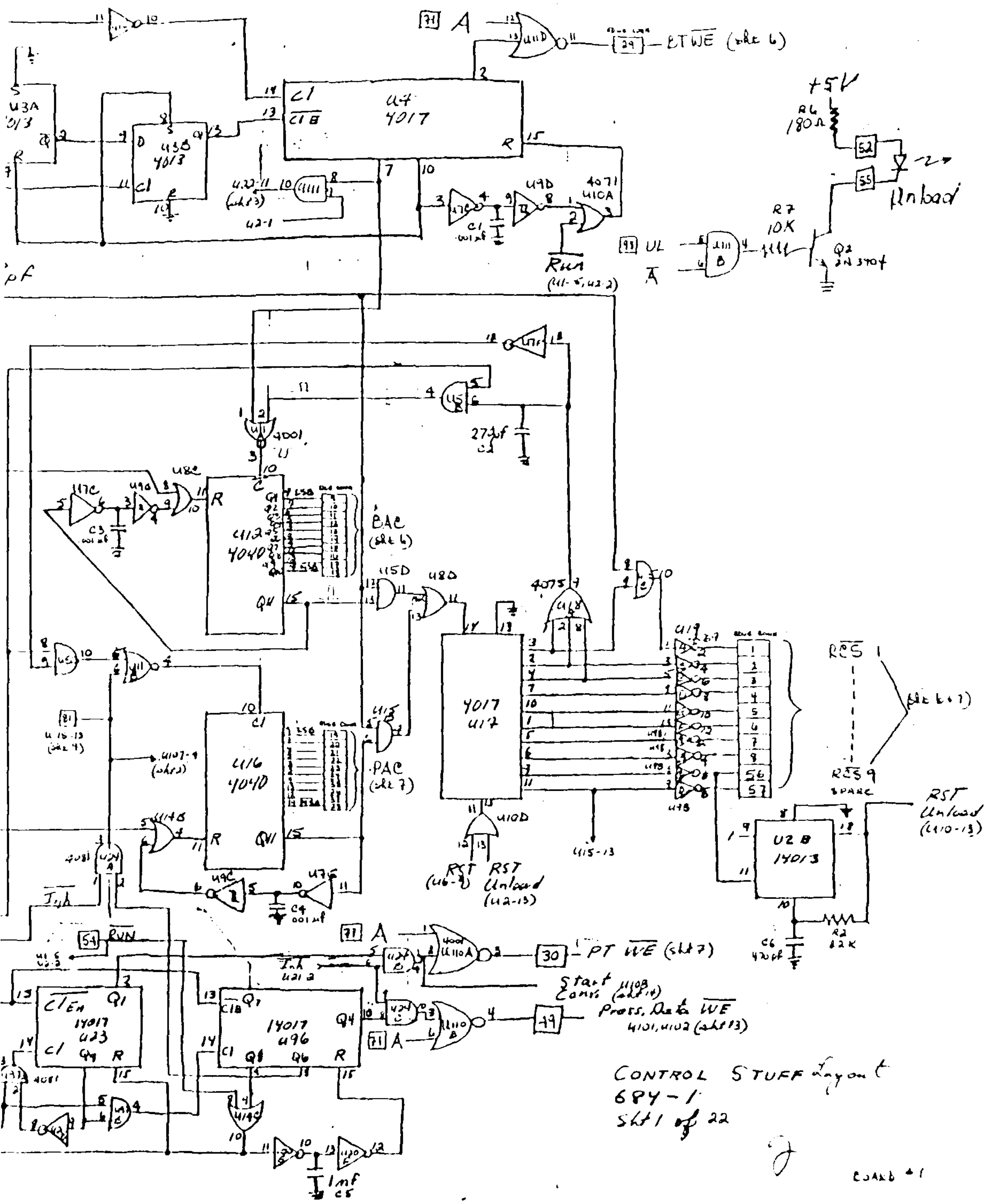

CONTROL STUFF Layout
684-1
Sht 1 of 22

Board #1

END

DATE
FILMED

8-86

DTIC